On the history of the early meteoritic bombardment of the Moon: was there a terminal lunar cataclysm?

Greg Michael[1], Alexander Basilevsky[1,2], Gerhard Neukum[1]

[1]Freie Universitaet Berlin, Malteserstr., 74-100, Haus D, 12249 Berlin Germany;

[2]Vernadsky Institute of Geochemistry and Analytical Chemistry, RAS, Kosygin Str., 19, 119991 Moscow

Abstract

This work revisits the hypothesis of the so-called 'lunar terminal cataclysm' suggested by Tera et al. (1973, 1974) as a strong peak in the meteorite bombardment of the Moon around 3.9 Ga ago. According to the hypothesis, most of the impact craters observed on the lunar highlands formed during this short time period and thus formed the majority of the lunar highland impact breccias and melts. The hypothesis arose from the observation that the ages of highland samples from all the lunar missions are mostly grouped around 3.9–4.0 Ga. Since those missions, however, radiometric dating techniques have progressed and many samples, both old and new, have been re-analyzed. Nevertheless, the debate over whether there was a terminal cataclysm persists. To progress in this problem we summarized results of 269 K-Ar datings (mostly made using the ^{40}Ar-^{39}Ar technique) of highland rocks represented by the Apollo 14, 15, 16, 17 and Luna 20 samples and 94 datings of clasts of the highland rocks from 23 lunar meteorites representing 21 localities on the lunar surface, and considered them jointly with the results of our modelling of the cumulative effect of the impact gardening process on the presence of impact melt of different ages at the near-surface of the Moon.

The considered results of K-Ar dating of the Apollo-Luna samples of lunar highland rocks confirmed a presence of strong peak centered at 3.87 Ga. But since the time when the hypothesis of terminal cataclysm was suggested, it has become clear that this peak could be a result of sampling bias: it is the only prominent feature at the sites with an apparent domination of Imbrium basin ejecta (Apollo 14 and 15) and the age pattern is more complicated for the sites influenced not only by Imbrium ejecta but also that of other basins (Nectaris at the Apollo 16 site and Serenitatis at the Apollo 17 site). Our modeling shows that the cataclysm, if it occurred, should produce a strong peak in the measured age values but we see in the considered histograms and relative probability plots not only the 3.87 Ga peak (due to Imbrium basin), but also several secondary peaks caused by the formation of other basins distributed between 3.87 and 4.25 Ga.

The lunar terminal cataclysm hypothesis is in disagreement with the distribution of K-Ar ages for the highland rocks of the lunar meteorites. The population of lunar meteorites representing localities randomly distributed over the lunar surface, and thus free from the mentioned sampling bias, shows no ~3.9 Ga peak as it should, if the cataclysm did occur.

We conclude that the statistics of sample ages contradict the terminal cataclysm scenario in the bombardment of the Moon. We also see evidence for the formation of several impact basins between 3.87 and 4.25 Ga which is likewise incompatible with the hypothesis of a short interval cataclysm. There remain other basins, including the largest South Pole – Aitken, the ages of which should be determined in future studies to further clarify the impact hostory. Sample-return missions targeted to date several key basins need to be planned, and the continued study of lunar meteorites may also bring new details to the general view of the impact bombardment of the Moon.

Keywords

Moon, surface; regoliths; impact processes; cratering

1. Preface

This work was started some years ago at the initiative of Professor Gerhard Neukum, of Freie Universitaet Berlin, who sadly passed away in 2014. He discussed the early results with great enthusiasm, suggesting new approaches, and writing and editing pieces of the evolving manuscript. Despite the long interval to publication, we acknowledge his significant contribution to the present work as a coauthor.

2. Introduction

This paper considers the issue of the terminal lunar cataclysm which is a potential feature of so-called early intense bombardment. The latter concept in relation to the Moon was first suggested even before the Apollo-Luna sample returns: Hartmann (1965, 1966), by combining terrestrial and lunar crater counts, estimated the age of the lunar maria to be 3.6 Ga. Applying the accepted assumption of the time, that the Moon was about 4.7 Ga old, and considering the observed significantly higher density of craters in lunar highlands, he concluded that in pre-mare time the cratering rate on the Moon had to be roughly two hundred times the average post-mare rate. Isotopic measurements of absolute ages of samples of lunar rocks returned by the Apollo and Luna missions confirmed this prediction (e.g., Papanastassiou and Wasserburg, 1972; Hartmann, 1972; Turner et al., 1973; Neukum et al.,

1975; Turner, 1977). Some of these works considered the early intense bombardment as the final stages of planetary accretion with the bombardment rate decreasing with a half-life of $\leq 10^8$ years (e.g., Hartmann, 1972), while others considered it to be the result of large collisions in the asteroid belt (e.g., Turner et al., 1973). Photogeologic analysis of images of Mercury, Mars, as well as planetary satellites and asteroids showed that the early intense bombardment was a phenomenon which occurred throughout the inner Solar System.

The ‘lunar terminal cataclysm’ hypothesis is one possible element of the early intense bombardment. It suggests that approximately 3.9 Ga ago there was a strong peak in the bombardment of the Moon when most of the craters now observed in the lunar highlands, and thus most of the lunar highland impact breccias, were formed (Tera et al., 1973, 1974). It is based on the observation that the highland samples, which were brought back by the various lunar missions, have ages determined by a variety of isotopic techniques that are grouped around 3.9–4.0 Ga. This is considered evidence for widespread shock metamorphism and element redistribution resulting from large-scale impacts on the Moon during that relatively narrow time interval. Since its first publication, the hypothesis and variants of it have been widely discussed with both *pro* and *contra* arguments (e.g., Baldwin, 1974; Hartmann, 1975; Grinspoon, 1989; Neukum, Ivanov, 1994; Cohen et al., 2000; Stoffler, Ryder, 2001; Hartmann, 2003; Chapman et al., 2007; Hartmann et al., 2007; Bottke et al., 2012; Geiss, Rossi, 2013; Morbidelli et al., 2012; Fernandes et al., 2013; Norman, Nemchin, 2014; Frey, 2016; Boehnke, Harrison, 2016). In particular, it has been argued more recently that it is problematic to reconcile the apparent late timing of basin formation with the decay of accretional leftovers (Ryder, 2002; Bottke et al., 2007) spurring new interest in the idea that they could have been produced during a late 'spike' from a differenct source.

In this paper we consider whether or not a lunar terminal cataclysm occurred. With this purpose, we first survey and analyze the published results of K-Ar dating of lunar highland rocks: the Apollo 14-17 and Luna-20 samples and the lunar meteorites. Figure 1 shows the localities of the Apollo and Luna landing sites from which samples of lunar materials were returned to Earth. Then we model the presently observed distribution of ages of impact products in the surface layer of the Moon for a scenario where the early intense bombardment declined gradually, and for another where a terminal cataclysm occurred. Finally, we consider the results of our analyses and discuss the considerations of this problem made by other authors.

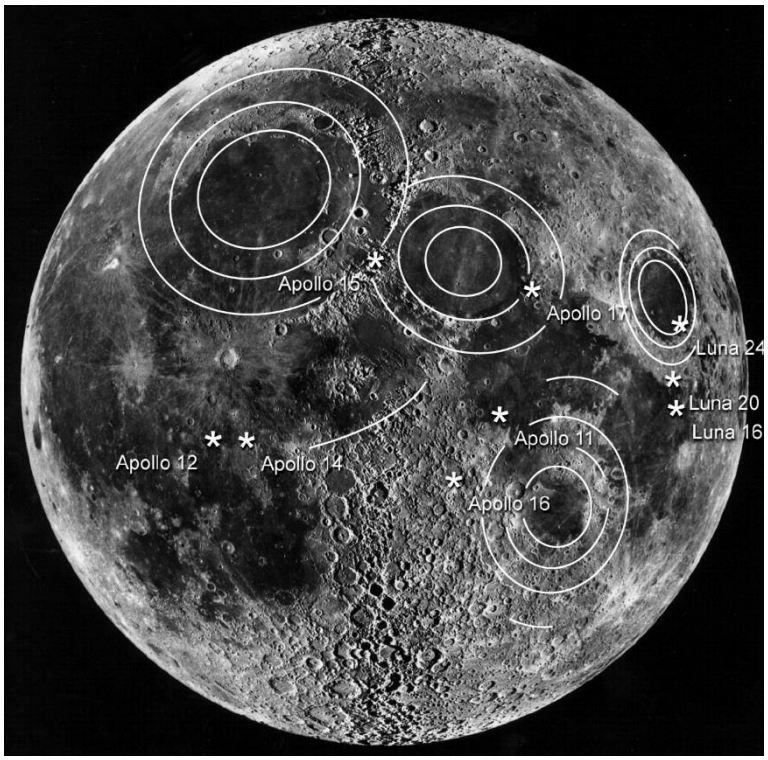

Figure 1. Apollo 11-17 and Luna 16-24 landing sites on a background mosaic of telescopic images of the Moon taken at the Lick Observatory. The rings of the Imbrium, Serenitatis, Nectaris and Crisium basins are shown as they were mapped by Wilhelms and McCauley (1971).

3. Summary of K-Ar dating of lunar highland rocks

Here we consider the results of K-Ar dating of samples of lunar highland rocks, including both Apollo and Luna samples and lunar meteorites. In this work, we refer to the data collectively as K-Ar measurements, after the underlying physics, although most were made using the Ar-Ar method. The K-Ar clock is easily reset by thermal events so that K-Ar dating is highly sensitive to shock metamorphism and impact melting resulting from meteoritic bombardment (e.g., McDougall and Harrison, 1999; Flude et al., 2014; Jourdan et al., 2014; Wartho et al., 2014). Three major sources of information for the considered samples and their ages were used. The first was *The Lunar Sample Compendium* compiled by Charles Meyer at the NASA Johnson Space Center, Houston, Texas (http://curator.jsc.nasa.gov/lunar/compendium.cfm). It contains information on ~360 lunar samples collected by the Apollo astronauts and on a few samples retrieved by the Luna 16, 20, and 24 robotic sample return missions. For each sample it gives a reference number which also specifies on which mission it was retrieved, its mass, and a short description of the place of its collection, its petrology, mineralogy, chemistry, isotopic dating and other studies as well

as photos of the sample and a list of supporting references. The second source was *The Lunar Meteorite Compendium* compiled by Kevin Righter, also at the NASA Johnson Space Center, Houston (http://curator.jsc.nasa.gov/antmet/lmc/index.cfm). The third source was the *List of Lunar Meteorites*, maintained by Randy Korotev, Washington University in St. Louis (http://meteorites.wustl.edu/lunar/moon_meteorites_list_alumina.htm). The meteorite compendia contain essentially the same type of information as *The Lunar Sample Compendium*. Additionally, we consulted publications on specific samples not covered by the mentioned compendia.

To understand the details of the dating and its results, we traced the age data from the compendium to the original publications. For the dating results published before the new constants for K decay (Steiger and Jager, 1977), we applied the necessary corrections if not already included in the compendium.

We considered lunar highland breccia samples and components of them, for which small and very small subsamples were used for dating. In different works on dating, different subsamples of the same hand-sample were used. Keeping in mind that different parts of breccias may have their own provenance, we considered ages determined for different subsamples as independent age values and included them separately in the appropriate tables and histograms. When the same sample was analyzed in several works, we took the age value with the smallest error bars. For example, the Ar-Ar age for the anorthosite 15415 was measured by Husain et al. (1972) as 4.09 ± 0.19 Ga, by Turner et al. (1972) as 4.05 ± 0.15 Ga, and by Stettler et al. (1973) as 3.99 ± 0.06 Ga. We included in our consideration the latter value. In a recent work, Fernandes et al. (2013) reported that in studying some samples of Apollo 16 and 17 highland rocks, they were able to measure up to three ages: 1) a maximum age which is probably the crystallization age, 2) the time of an early impact reset event, and 3) the time of the latest impact reset event. In our consideration we considered the second and the third age values as independent measurements and included them as such in the histograms.

Following the descriptions in the compendium and in the original publications, we subdivided the samples under study into three types: impact-melt breccias, fragmental (no-melt) breccias, and rocks with igneous structures. There is general consensus that all samples of highland rocks represent clasts in impact breccias. A consideration of the ages is given first separately for each landing site where highland rocks were collected: for Apollo 14 through to Apollo 17, plus Luna 20, and then we consider the K-Ar ages of the highland rock components of lunar meteorites. Finally, we summarize the results of all considerations.

Figure 2 shows a set of histograms of the considered ages for the highland rocks sampled by the Apollo 14–17 and Luna 20 missions (269 datings). Tables with the age and other data for the considered samples as well as histograms showing the distribution of ages for different rock lithologies for different sites are given as supplementary materials.

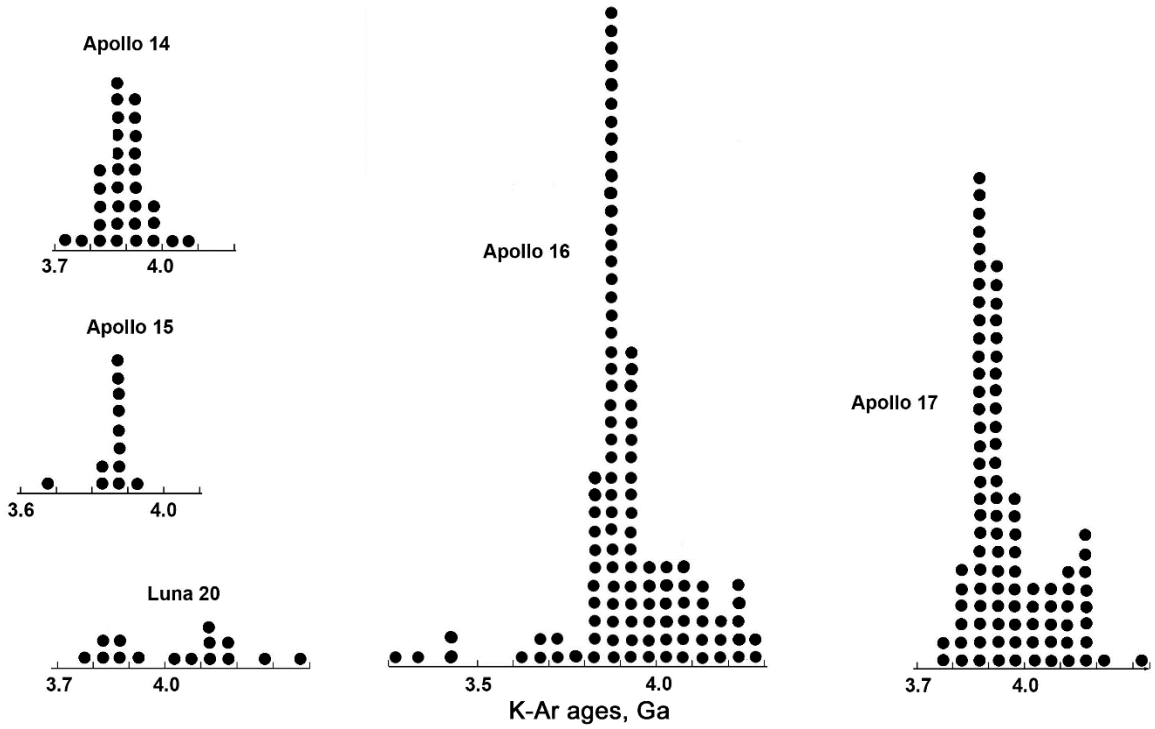

Figure 2. Histograms of the considered K-Ar ages of lunar highland rocks of the Apollo-Luna returned samples.

3.1. Apollo 14 ages of highland rocks

Apollo 14 landed at 3.65º S, 17.47º W within the hypsometrically low non-mare area about 50 km north of the 80-km crater Fra Mauro. The surface rocks of this area belong to the Fra Mauro formation which is considered to be the ejecta from the Imbrium impact basin with an admixture of local materials (Spudis and Pieters, 1991 and references therein). The site is 550 km south of Montes Carpatus (Figure 3a), the south topographic rim of Imbrium basin and the suggested boundary of its excavation cavity (Wilhelms, 1987). The area is characterized by low ridges separated by valleys radiating from the Imbrium basin. The spacecraft landed in a broad shallow valley between the ridges on an undulating surface covered by numerous small craters whose ejecta form the local regolith (Chapman et al., 1971) (Figure 3b). The crew investigated the close vicinity of the landing site and terrain along the 2 km-long route to the rim of the morphologically fresh 340-m Cone Crater. The

major rock types sampled at this site are impact breccias, rich in so-called KREEP material derived from the Imbrium basin cavity (e.g., LSPET, 1971; Taylor et al., 1991).

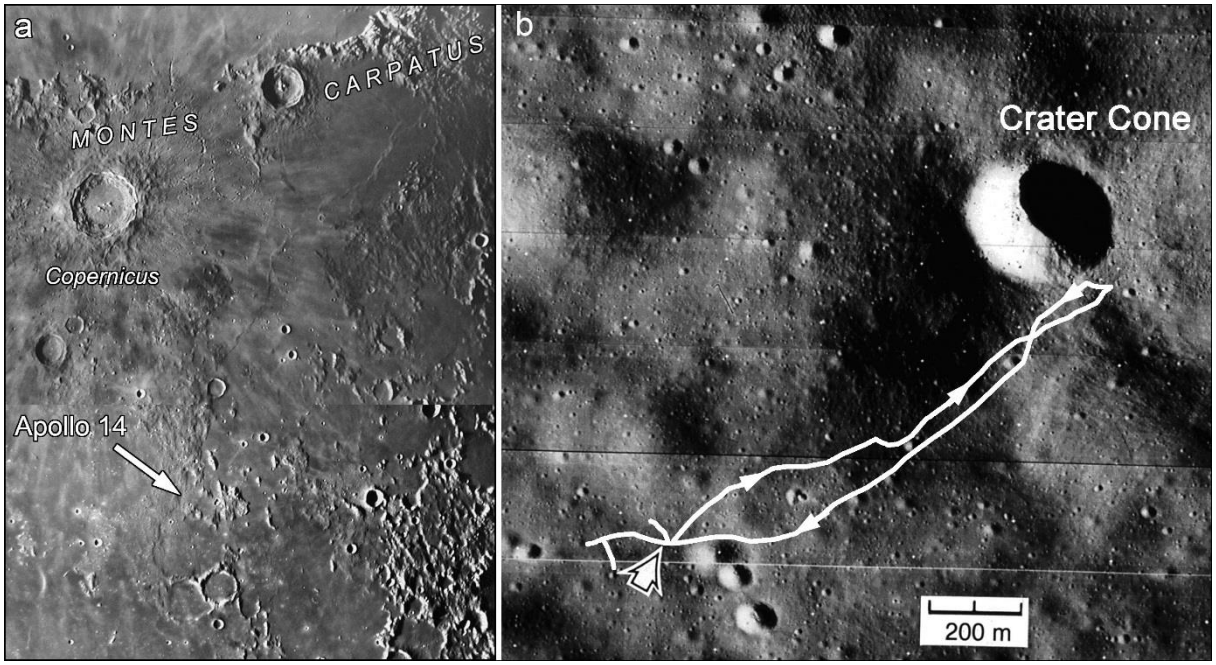

Figure 3. The Apollo 14 landing site: a) Mosaic of images e16 and e18 from the Consolidated Lunar Atlas (http://www.lpi.usra.edu/resources/cla/); b) The LO-3 image is from http://www.lpi.usra.edu/lunar/missions/apollo/apollo_14/images/a14_lsite4_lg.gif. The traverse is from http://www.nasm.si.edu/collections/imagery/apollo/FIGURES/traverses/as14traverse.jpg. Black and white arrow shows the position of the lander.

We acquired 31 determinations of K-Ar age for the Apollo 14 highland rocks from the *Lunar Sample Compendium* and associated literature (Figure 2 and also Figure 1S and Table 1S in supplementary materials). Among them, 25 are impact melt breccias, 2 are no-melt breccias, and 4 are rocks with igneous structures (anorthosite and gabbro-norite). The impact melt breccias show a range of ages from 3.73 to 4.09 Ga with a prominent peak between 3.8 and 3.9 Ga (Figure 1Sa). The no-melt (granulitic) breccias have ages of 3.97 and 4.00 Ga, and the rocks with igneous structures have ages from 3.85 to 3.92 Ga (Figures 1Sb and 1Sd, correspondingly).

It is seen from Figure 2 and 1S that the distribution of K-Ar ages of the Apollo 14 rocks which are considered to be ejecta from the Imbrium basin shows a strong peak around ~3.9 Ga. This is also observed for impact melt breccias, which make up the majority of analyses (Figure 1Sa). The ages of the two samples of no-melt breccias show a small shift to

older ages compared to this peak (Figure 1Sb). A summary histogram for the impact melt and no-melt breccias shows a prominent peak around ~3.9 Ga (Figure 1Sc). The ages of the four samples of rocks with igneous structures are in the center of this peak (Figure 1Sd). These results are in agreement with the majority of works dating the formation of Imbrium basin as 3.8-3.9 Ga (e.g., Wilhelms, 1987; Stoeffler and Ryder, 2001; Stoeffler et al., 2006). The fact that the ages of the four samples of the rocks with igneous structures coincide with the 3.8-3.9 Ga peak suggests that although these rocks preserved the igneous structures, their ages were probably reset by the Imbrium-forming event. The alternative possibility, that these are ages of their crystallization from the magma closely before the basin-forming impact, cannot be excluded. The few younger ages probably record resets by post-Imbrium impacts and a couple of the older ages (4.00 ± 0.02 and 4.09 ± 0.02 Ga) probably record pre-Imbrium events.

3.2. Apollo 15 ages of highland rocks

Apollo 15 landed at 26.13º N, 3.63º E on the mare surface at the eastern margin of the Imbrium basin (Figure 4a) inside the basin's topographic rim represented here by Montes Apenninus (Spudis and Pieters., 1991 and references therein). The astronauts using the Lunar Roving Vehicle made three study traverses, two of which reached the lower parts of the slope of the Apenninus massif (Figure 4b). Samples taken at the massif were expected to provide the material ejected by the basin event from a deeper level in the lunar crust than that sampled in the Fra Mauro Formation by Apollo 14. However, fewer samples than expected were obtained from the massif. Most of those collected were small and of uncertain geologic context because the outcrops were covered by thick colluvium (Swan et al., 1972; LSPET, 1972; Wilhelms, 1997).

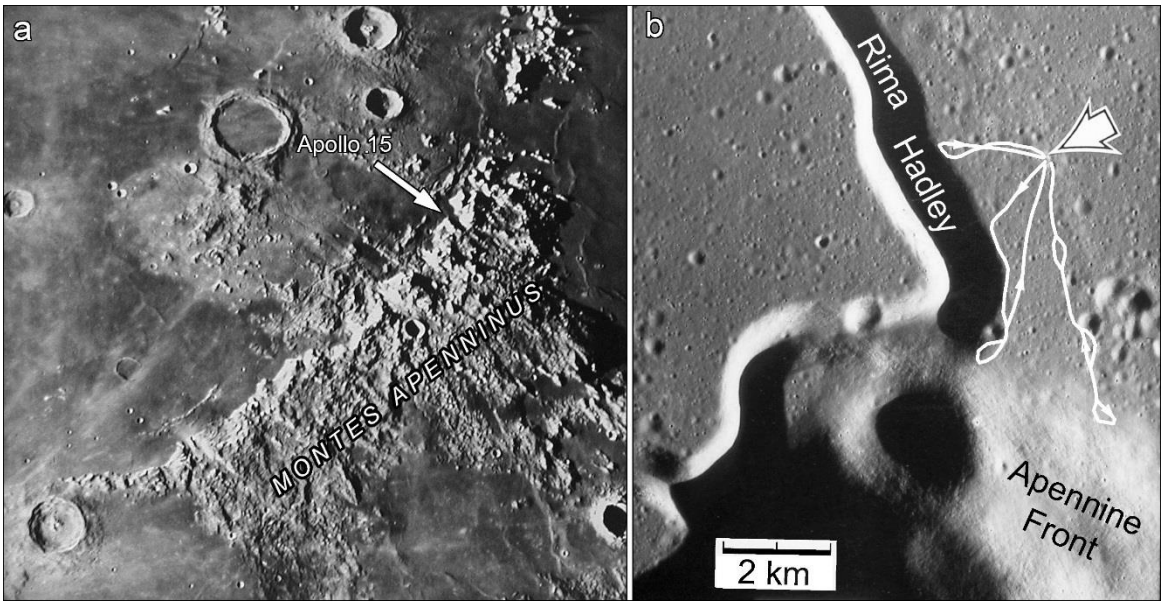

Figure 4. Landing site of Apollo 15: a) Image c11 from the Consolidated Lunar Atlas (http://www.lpi.usra.edu/resources/cla/); b) The Apollo 15 image is from http://www.lpi.usra.edu/lunar/missions/apollo/apollo_15/images/vertical_hi_lg.gif. The traverse map is from http://www.nasm.si.edu/collections/imagery/apollo/FIGURES/traverses/as15traverse.m.jpg. Black and white arrow shows the position of the lander.

We acquired only 12 determinations of K-Ar age for the Apollo 15 highland rocks from the *Lunar Sample Compendium* and the associated literature (Figure 2 as well as Figure 2S and Table 2S in supplementary materials). Among them, 8 are impact melt breccias, one is a no-melt breccia, and three are rocks with igneous structures (anorthosite and gabbro-norite). The impact melt breccias show a range of ages from 3.68 to 3.87 Ga with a prominent peak between 3.85 and 3.9 Ga. The no-melt (granulitic) breccia has an age of 3.94 Ga, and the rocks with igneous structures have ages from 3.83 to 3.90 Ga.

It is seen from Figures 2 and 2S that the distribution of K-Ar ages of the Apollo 15 rocks, which are likewise considered to be ejecta from the Imbrium basin, also shows a strong peak close to 3.9 Ga both for the whole set of samples studied and for the impact melt breccias, which make up the majority of analyses. The age of the sample of no-melt (granulitic) breccia is somewhat older, but within the mentioned peak. As for the Apollo 14 samples, the ages of the three samples of rocks with igneous structures coincide with the peak. Again, these results are in agreement with the majority of works dating the formation of Imbrium basin as 3.8-3.9 Ga (e.g., Wilhelms, 1987; Stoeffler and Ryder, 2001; Stoeffler et al., 2006). The youngest value of our sample of ages (3.67 ± 0.09 Ga) probably records a reset by a post-Imbrium impact and one slightly older age (3.94 ± 0.06 Ga) overlaps with the peak in its error bars so it may either be part of the peak or record some pre-Imbrium event.

3.3. Apollo 16 ages of highland rocks

Apollo 16 landed at 8.97º S, 15.5º E in the Descartes mountain region 60 km west of the Kant Plateau, a part of the Nectaris basin rim (Figure 5a). Two geologic units were sampled by this mission: the Cayley and Descartes Formations (Muehlberger et al., 1973; Wilhelms, 1987; Spudis and Pieters., 1991 and references therein). The first one forms the Cayley plains widespread in the highlands of the central part of the nearside of the Moon. Before the Apollo 16 mission these plains were thought to be composed of volcanic lavas, but the returned samples showed that the Cayley material is made up of impact breccias (LSPET,

1972) being probably a mixture of ejecta from Imbrium basin and local materials (Wilhelms, 1987 and references therein). The Apollo 16 Lunar Module landed on the Cayley plains (Figure 5b). The Descartes Formation at the site is represented by Stone Mountain and Smoky Mountain standing about 1 km above the plain. The material of the Descartes formation is considered by Wilhelms (1987) to be Nectaris-basin deposits modified by Imbrium secondary craters and ejecta flows although other suggestions have also been discussed (see below).

Ejecta from two craters at the landing site, South Ray crater and North Ray crater, strongly affected the mission sampling (Muehlberger et al., 1973). The ejecta of South Ray crater (700 m in diameter and 120 m deep), which is superposed on the Cayley plains, affected the southern part of the study traverse including the sampled lower part of the Stone Mountain slope. North Ray crater (~1 km in diameter and 230 m deep) is at the foot of Smoky Mountain and probably excavated the materials not only of the Cayley formation, but of the underlying Descartes formation, too (Spudis and Pieters, 1991 and references therein). The astronauts using the Lunar Roving Vehicle made three study traverses, one of which reached the lower part of the Stone Mountain and another approached the base of Smoky Mountain (Figure 5b).

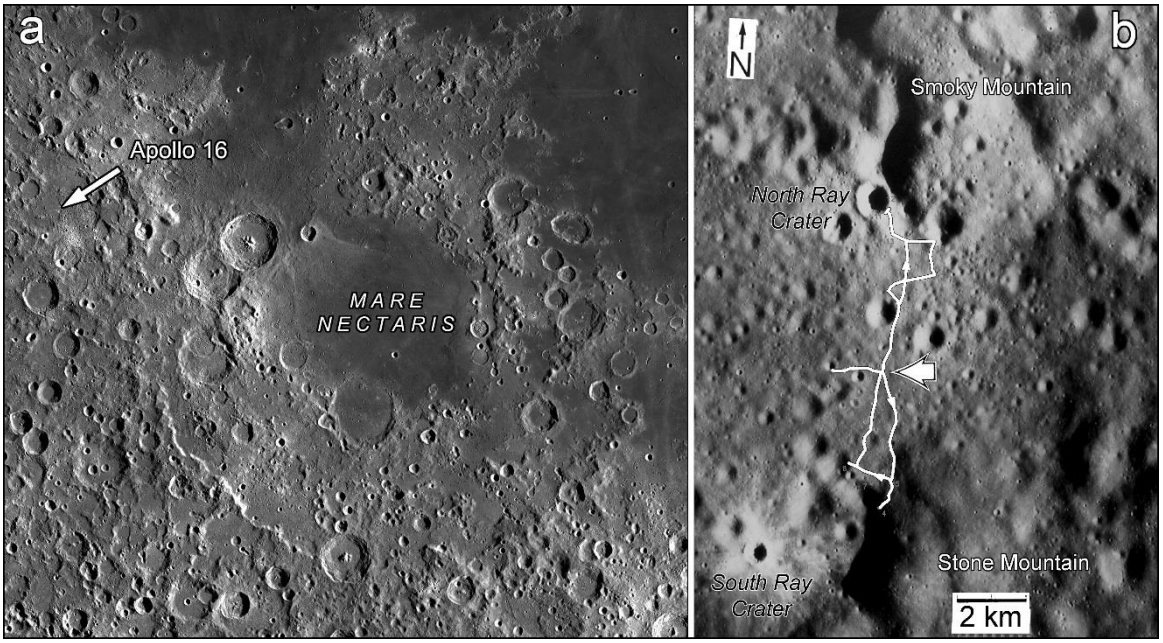

Figure 5. Landing site of Apollo 16; a) LROC WAC mosaic, courtesy of NASA/ASU; b) The Apollo 16 image http://www.lpi.usra.edu/lunar/ missions/apollo/apollo_16/images/vertical_hi_res_lg.gif. The traverse map is from http://www.nasm.si.edu/collections/imagery/apollo/FIGURES/traverses/as16traverse.m.jpg. Black and white arrow shows the position of the lander.

We acquired from the Lunar Sample Compendium and the associated literature 112 determinations of K-Ar age for the Apollo 16 highland rocks (Figure 2 as well as Figure 3S and Table 3S in Supplementary materials). Among them, 41 are impact melt breccias, 41 are no-melt breccias, and 30 are rocks with igneous structures (anorthosites, gabbroic anorthosites and anorthositic gabbro). The impact melt breccias show a range of ages from 3.75 to 4.29 Ga with a prominent peak between 3.85 and 3.90 Ga. The no-melt (mostly clastic) breccias have ages between 3.30 and 4.19 Ga with two peaks at 3.85-3.95 and 4.05-4.15 Ga, and the rocks with igneous structures have ages from 3.43 to 4.25 Ga with three low peaks at 3.85-3.90, 4.0-4.1 and 4.20-4.25 Ga. The summary histogram shows a prominent peak at 3.85-3.95 Ga, a shoulder at 3.95 to 4.10 Ga and a minor peak at 4.20-4.25 Ga.

The age histogram for Apollo 16 shows that the boundary between the prominent peak at 3.85-3.95 Ga (which was also seen on the Apollo 14 and 15 age histograms) and the shoulder-and-peak of older ages is near 4.0 Ga. We examined where samples were taken which have ages greater or lesser than 4 Ga (see Table 1). At the Apollo 16 site, the samples for which we consider the ages were taken in three areas: 1) within the ejecta blanket of North Ray Crater which, as was mentioned above, probably excavated materials of the Cayley and Descartes Formations; 2) in the vicinity of the Lunar Module (LM), midway between North Ray and South Ray craters; and 3) within the ejecta blanket of South Ray Crater, which probably mainly excavated material of the Cayley Formation. The data of Table 1 show that samples having ages > 4 Ga appear to relate to the Descartes material.

Table 1. Areal distribution of samples with ages older and younger than 4 Ga at the Apollo 16 site.

Area	Number of samples with age > 4 Ga	Number of samples with age < 4 Ga	Total
Ejecta of North Ray crater	23	39	62
LM vicinities	4	17	21
Ejecta of South Ray crater	1	28	29
All areas	28	84	112

The spatial association of the older age samples with North Ray Crater had been noticed in several works which also considered the specifics of chemical composition of the older and younger highland materials at the Apollo 16 site. For example, Maurer et al. (1978) distinguished two groups of samples, one having ages 4.025–4.11 Ga and another one with

ages 3.76–3.93 Ga (recalculated values). They noted that the older group of samples is spatially associated with ejecta from the North Ray crater and concluded that in this location there is an older anorthositic breccia overlain by a younger breccia. They also found that the samples with older ages contain <100–300 ppm of K, have low REE abundances and strong positive europium anomalies, while the samples with the younger ages contain 1000–3000 ppm of K, have high REE abundances and strong negative europium anomalies. The chemical characteristics of the latter group are typical of KREEP materials which, since the Apollo 14 mission, have been considered typical of ejecta from the Imbrium basin (e.g., LSPET, 1971).

These observations were confirmed by Stoeffler et al. (1985) who reported on the studies made by the "North Ray Crater Consortium". As a result of analyses of 187 samples (including individual coarse grains from the soils) taken at Stations 11 and 13, which are within the ejecta blanket of North Ray Crater, these authors concluded that the lower part of the material excavated by this crater is a megabreccia with clasts of highly feldspathic KREEP-free breccias interpreted to represent the Descartes Formation. The upper part contains KREEP-bearing polymict breccias and appears to be similar to the lithologies found in the Cayley plains.

This chemical specifics of the Descartes and Cayley Formations were then described by Korotev (1994) who distinguished two major chemical trends in the Apollo 16 melt rocks, classed as eastern or western. The eastern trend is represented by melt rocks which are feldspathic, poor in incompatible and siderophile elements, and appear to have provenance in the Descartes formation to the east of the site. The western trend is represented by relatively mafic, KREEP-bearing breccias, which are a major component of the Cayley plains to the west of the site.

Norman et al. (2006) determined the K-Ar ages of the Apollo 16 impact melt rocks considering their results according to the chemical groups of Korotev (1994). Among 25 studied samples collected at different stations, 20 fall in the age range 3.75–3.96 Ga, one showed an age of 4.19 Ga and four samples could not be dated. Interestingly, the oldest sample is a highly aluminous breccia with very low abundances of incompatible lithophile trace elements derived from the ejecta of North Ray Crater. However another sample representing this chemical group and collected in the same locality showed the age 3.895 Ga.

The literature reveals a great diversity of opinions about the provenance of the Cayley and Decartes Formations, their absolute ages and their relation to specific basin-forming events. Schaeffer and Husain (1973), who first provided evidence for the older K-Ar ages (4.03–4.16, when recalculated) for fragments from the Apollo 16 soils, did not connect these

ages to any specific events. They considered the suite of samples with younger ages (3.86–3.96 Ga) as dating the Cayley Formation which, in their opinion, could be debris from the Imbrium, Nectaris or Orientale basins.

Maurer et al. (1978) considered that the younger materials represent the ejecta of one or more basin-forming events (Imbrium and/or others, including the spatially closest Nectaris), while the older materials represent the ejecta of medium-sized craters large enough to reset the ages of the original anothositic crust but too small to excavate the KREEP-rich layer beneath the crust. In their model, Maurer et al. (1978) relate the KREEP genesis to a deep crustal layer that was excavated only by large-scale basin-forming impacts. However the later gamma-ray and neutron spectroscopy survey showed that KREEP material is certainly not associated with the Nectaris basin (see, for example, Figures 25 and 26 in Prettyman et al., 2006), so the suggestion of a Nectaris provenance for the younger Apollo 16 materials should be dismissed. Wetherill (1981) and Warren (2003) considered the group of samples with the age of ~4.1 Ga determined by Maurer et al. (1978) as an indication that this may be the age of the Nectaris basin.

Stoeffler et al. (1985) considered the results of their Ar-Ar (and Rb-Sr) dating of the Apollo 16 samples with high spectral resolution using 15 gas extraction steps. They stated that the lower resolution spectra tend to lead to the higher ages and noted that Maurer et al. (1978) usually used nine steps. Stoeffler et al. (1985) , however, found two plateaus (of excellent quality) with ages lower and higher than 4 Ga for each of two samples (cataclastic anorthosite 67536 and microporphyritic melt breccia 67715). They explained the higher age, 4.08 Ga, for sample 67715 by saying that it retained information from its “prior history”. The authors concluded that the Nectaris basin age is probably 3.85± 0.05 Ga and the Imbrium basin age is ~3.8 Ga. They also considered the the results of Rb-Sr dating of two samples of subophitic-ophitic impact melt rocks, one of which, 67559, showed an age of 3.84± 0.04 Ga while another, 67747, showed 3.94± 0.05 Ga. It is interesting that the older sample, the age of which was considered by Stoeffler at al. (1985) to be in the domain of Nectaris ages, is enriched in potassium (their Table 8) and thus is more likely of Imbrium provenance.

Norman et al. (2006), who did high-resolution measurements with 20–30 gas extraction steps, distinguished four petrologic groups among the 20 samples with ages between 3.75 and 3.96 Ga: 1) aluminous poikilitic, 3.749–3.793; 2) aluminous subophitic, 3.826–3.840; 3) mafic poikilitic, 3.852–3.877; and 4) troctolitic vitrophyre, dimict and metapoikilitic, 3.852–3.962 Ga. They considered them as formed in separate impact events but did not identify specific basins. The fifth petrologic group, highly aluminous breccia with

very low abundances of incompatible lithophile trace elements, is represented by two samples, one showing an age of 3.895 Ga and another one (mentioned above) showing 4.190 Ga.

So, the above consideration shows that the majority of researchers agree that some of the Apollo 16 samples are derived from the Cayley Formation. They show the presence of KREEP material and most probably represent distant ejecta from the Imbrium basin with an admixture of local materials. In the data we collated, these samples are responsible for the most prominent 3.85–3.95 Ga peak, which probably dates the Imbrium event. There is little doubt that others of the Apollo 16 samples derive from the Descartes Formation. They are highly feldspathic with a deficit of elements typical of KREEP material. In the data collated by us these samples are responsible for the ages older than 4 Ga, which probably correspond to Nectaris and maybe some other event(s). This statement is in agreement with those of Wetherill (1981) and Warren (2003) mentioned above, that the group of samples with ages of ~4.1 Ga may record the formation of the Nectaris basin. The 4.15–4.25 Ga peak seen in our Figure 2 probably dates some pre-Nectaris event. Recent works by Norman & Nemchin (2014) and Norman et al. (2016) report on the noritic anorthosite 67955 which, based on its petrological and geochemical characteristics and the results of ^{147}Sm-^{143}Nd and U-Pb dating, is a well crystallized melt produced by an impact in the Procellarum-KREEP terrane ~4.22 Ga ago, later transported as a rock fragment to the Apollo 16 site as Imbrium ejecta.

3.4. Apollo 17 ages of highland rocks

The Apollo 17 landing site is at 20.19ºN 30.77ºE at a highland/mare boundary near the southeastern rim of the Serenitatis basin (Figure 6a). The spacecraft landed on the floor of inter-mountain Taurus-Littrow Valley filled by mare basalts and the astronauts made three study traverses using the Lunar Roving Vehicle, in which they reached the bases of three landforms of the highland terrain: South Massif, North Massif and the Sculptured Hills (Figure 6b), where samples of highland materials were collected. These two mountain massifs and the knobby terrain of the hills have, since the Apollo times, usually been considered to represent the ejecta of the Serenitatis basin with an admixture of Imbrium basin ejecta (Wilhelms, 1987; Spudis and Pieters, 1991 and references therein). However Spudis and Ryder (1981) noticed that the typical knobby terrain of the Sculptured Hills is broadly distributed to the east of Mare Serenitatis and overlies large craters (including Le Monnier) that are superposed on the Serenitatis basin rim, so the Sculptured Hills terrain should be of post-Serenitatis age. This interpretation was later supported by photogeologic analysis

involving LROC WAC images which in particular showed that the lineations of this knobby terrain point back to Imbrium and thus the Sculptured Hills are probably a facies of the Imbrium basin ejecta (Spudis et al., 2011). This indirectly supports the earlier propositions that the Northern and Southern Massifs are to some degree influenced by ejecta from the Imbrium basin (Wilhelms, 1987; Spudis and Pieters, 1991). The highland material was also sampled within the so-called light mantle on the valley floor at the base of the South Massif. The light mantle is considered to be a deposit of an avalanche from the South Massif initiated by ejecta from Tycho crater (Spudis and Pieters, 1991 and references therein).

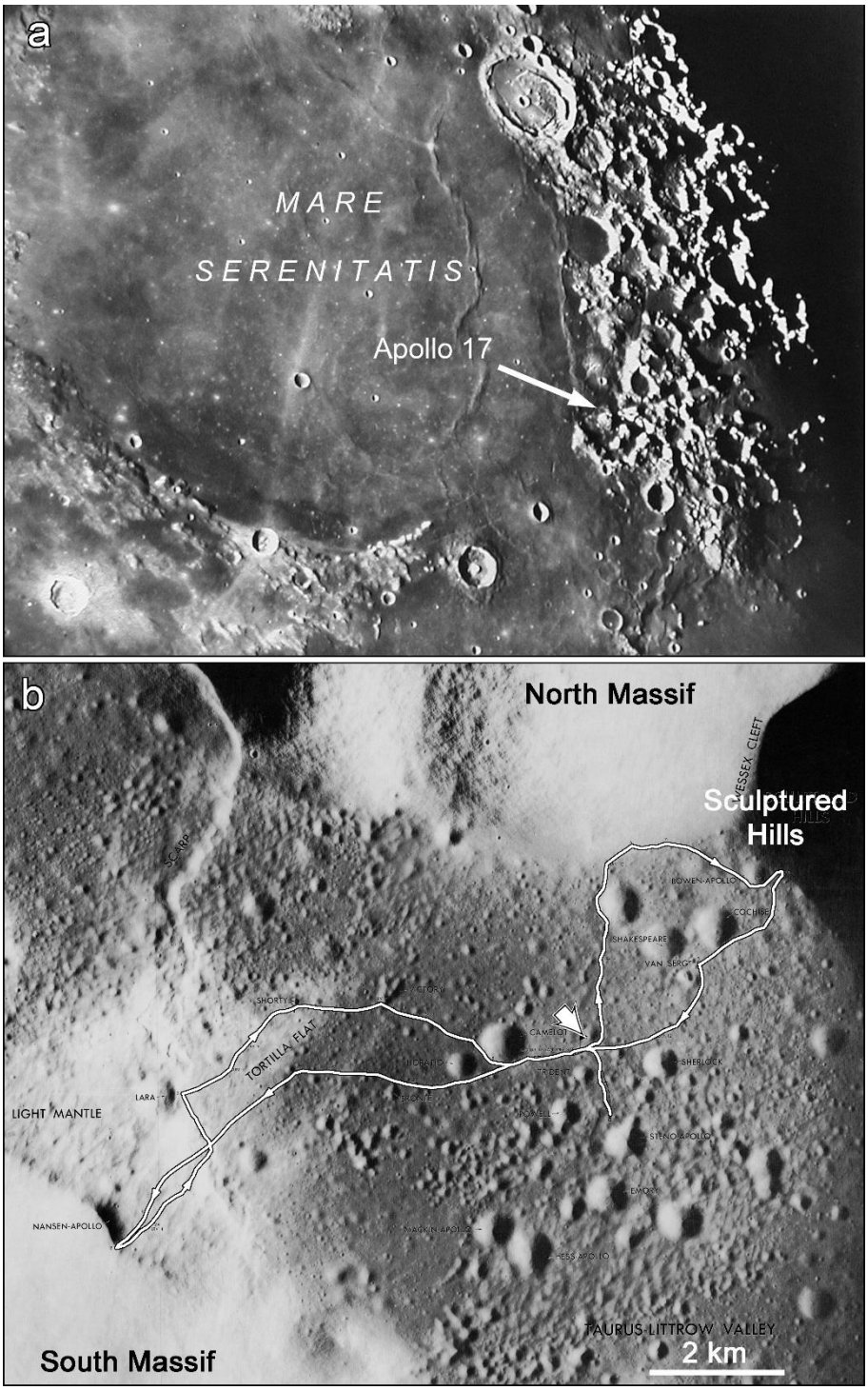

Figure 6. Landing site of Apollo 17. a) Image c6 from the Consolidated Lunar Atlas (http://www.lpi.usra.edu/resources/cla/); b) The image and the traverse map are from http://www.lpi.usra.edu/publications/slidesets/apollolanding/ApolloLanding/slide_37.html. Black and white arrow shows the position of the lander.

We acquired 96 determinations of K-Ar age for the Apollo 17 highland rocks from the *Lunar Sample Compendium* and associated literature (Figure 2 as well as Figure 4S and Table 4S). Among them, 36 are impact melt breccias, 47 are no-melt breccias, and 13 are rocks with igneous structures (gabbroic anorthosite, anorthositic gabbro, gabbro, troctolite, dunite). The

impact melt breccias show a range of ages from 3.81 to 4.14 Ga with a prominent peak between 3.85 and 3.90 Ga and a secondary peak between 4.05 and 4.10 Ga. The no-melt breccias (mostly with recrystallized and granulitic matrix) have ages between 3.79 and 4.23 Ga with a peak at 3.85–3.95 Ga and a minor peak at 4.15–4.20 Ga, and the rocks with igneous structures have ages from 3.86 to 4.33 Ga with a minor peak at 4.10–4.15 Ga. The summary histogram shows a prominent peak at 3.85-3.95 Ga and a noticeable peak at 4.1–4.2 Ga.

The results of K-Ar dating of the Apollo 17 samples were widely discussed in the literature. Kirsten and Horn (1974), who found an age of ~3.96 Ga for an anorthositic clast and two breccia samples and 4.18 Ga for a troctolite sample, were very cautious discussing their results. They stated that the observed age differences might be due to local events and not resolve the problem of the ages of the large impact basins. In relation to the latter they stated that the basins are older than ~3.8 Ga and that it is not possible to conclude whether they formed almost contemporaneously or were spread over the time interval of 4.6–3.8 Ga.

In many cases, the interpretations of K-Ar dating of the Apollo 17 samples were made under the obvious influence of the popular hypothesis of a terminal cataclysm (Tera et al., 1973, 1974). For example, Cadogan and Turner (1976) found the Ar-Ar age of the samples taken from the Station 6 boulder at the foot of the North Massif to be 3.86 ± 0.04 Ga, and considered this value, which is very close to the assumed age of Imbrium basin, to be the age of the Serenitatis basin. Jessberger et al. (1977) studying 17 subsamples of aphanitic impact melt breccia 73215 found the age range 3.83–4.18 Ga and concluded that the time of Serenitatis event is 3.92 ± 0.04 Ga, while values greater than 4 Ga are due to incomplete resetting. Oberli et al. (1979) found an age of 4.15 Ga for feldspathic granulitic impactite that they consider reliable, and suggest it as evidence of “a pre-cataclysm history”.

However, Schaeffer and Husain (1974) found an age range 3.43–4.33 Ga for pieces of the 2-4 mm fraction of the rake sample at Station 8 at the foot of Sculptured Hills, and suggested (involving data for the Apollo 16 sample 60025) that Orientale basin was formed ~3.85, Imbrium at ~3.95, Crisium and Humorum at ~4.05, and Nectaris at ~4.25 Ga. They proposed that the Serenitatis basin age should be >4.25 Ga. Fernandes et al. (2008, 2013) measured two Apollo 17 samples ages at ~4.2 Ga and considering these results together with the Apollo 16 samples they studied which also showed ages of ~4.2 Ga (see above), concluded that these are the ages of one or more basing forming events.

As for the analysis of the Apollo 16 K-Ar ages, we have examined whether there is a correlation between the measured ages of the Apollo 17 samples we considered, the locations where the samples were collected, and their potassium content. In relation to the highland

rock sampling within the Apollo 17 site one can distinguish three areas: 1) the area at the base of the North Massif, 2) the area at the base of Sculptured Hills, and 3) the area at the base of the South Massif (including the Light Mantle which is a landslide from the slope of the South Massif). Table 2 shows the distribution of samples with ages older and younger than 4 Ga among these areas.

Table 2. Areal distribution of samples with ages older and younger than 4 Ga at the Apollo 17 site.

Area	Number of samples with age > 4 Ga	Number of samples with age < 4 Ga	Total
Base North Massif	2	21	23
Base of Sculptured Hills	11	-	11
Base of South Massif	16	46	62
All areas	29	67	96

It can be seen from Table 2 that samples representing the materials of the North and South Massifs show ages both lower (dominant) and higher (subordinate, but essential) than 4 Ga, while all 11 samples collected from the lower part of the slope of Sculptured Hills show only ages greater than 4 Ga. As was mentioned earlier, the North and South Massifs are probably ejecta from the Serenitatis basin, while the morphology and age relations with post-Serenitatis craters suggest that Sculptured Hills are a facies of Imbrium ejecta. At first glance, this is in contradiction with the results for the Apollo 14, 15 and 16 samples considered above. If one considers the dating results for the samples derived from the North and South Massifs as a mixture of the Imbrium (<4 Ga) and Serenitatis (>4 Ga) ages, then why does the material representing the Imbrium landform show only ages >4 Ga?

The solution of this apparent problem may be in the high-velocity emplacement of the Imbrium ejecta, which formed the Sculptured Hills terrain. Based on the distance of this location from the Imbrium basin center (~1500 km) and assuming that the material was ejected under the angles from 15 to 45° above the horizon, one can calculate the velocity with which these ejecta were emplaced in the considered place was 1.3 to 1.4 km/s (Melosh, 1989, formula 6.1.1). Emplacement at this velocity should inevitably lead to mixing with the local materials, so one may suggest that the mentioned samples collected at the base of Sculptured Hills represent the admixture of the underlying Serenitatis material. One may also suggest that this is material of Imbrium ejecta whose K-Ar age was not reset by the ejection event. But we

do not see such non-reset material among the considered sets of samples, derived from the Apollo 14 and 15 landing sites, where the connection with Imbrium event is very obvious, so although presence of such material cannot be *a priori* ruled out, this is probably not the case.

The correlation between the K-Ar ages and the potassium content in the studied Apollo 17 samples looks different from what is observed for the Apollo 16 samples. Only two Apollo 17 samples picked up at the base of the Sculptured Hills have a potassium content as low as 30–40 ppm and an age >4 Ga. Most of the considered Apollo 17 samples, both with ages <4 Ga and >4 Ga, have more than 100–300 ppm of potassium, that is usually considered as resulting from an admixture of KREEP material. In the case of the Apollo 16 samples this was considered a signature of Imbrium derived material. This majority of the Apollo 17 samples derived from South and North Massifs, as was said above, seem to represent materials from Serenitatis with an admixture from Imbrium. If, however, we consider samples from this set with K-Ar age >4 Ga to represent Serenitatis materials, we must conclude that the latter are enriched in the KREEP component and this is not an exclusive feature of Imbrium materials. Indeed, the Serenitatis basin is adjacent to the region of KREEP terrain seen in the Lunar Prospector maps (Prettyman et al., 2006) and it may be possible that, at least, part of its ejecta is enriched in the KREEP component.

Finally, the above discussion leads us to conclude that the 3.85–3.95 Ga peak on the Apollo 17 summary histogram (Figures 2 and 4Se) dates the Imbrium basin while the 4.1–4.2 Ga peak could date the Serenitatis event.

3.5. Luna 20 ages of highland rocks

The Luna 20 sample return spacecraft landed in the highland area about 150 km south of Mare Crisium and about 30 km from the NE boundary of Mare Fecunditatis. The coordinates of the landing site were found to be 3.32° N, 56.33° E (http://www.laspace.ru/rus/luna20.html). Recently, after the Luna 20 lander had been identified in LROC NAC images, a more accurate determination of the coordinates led to the values 3.787° N, 56.625° E (http://www.lroc.asu.edu/news/index.php?/archives/210-LROC-Coordinates-of-Robotic-Spacecraft.html). Figure 7 shows the regional context of the Luna 20 landing site and a fragment of the LROC NAC image with the Luna 20 lander near the image center.

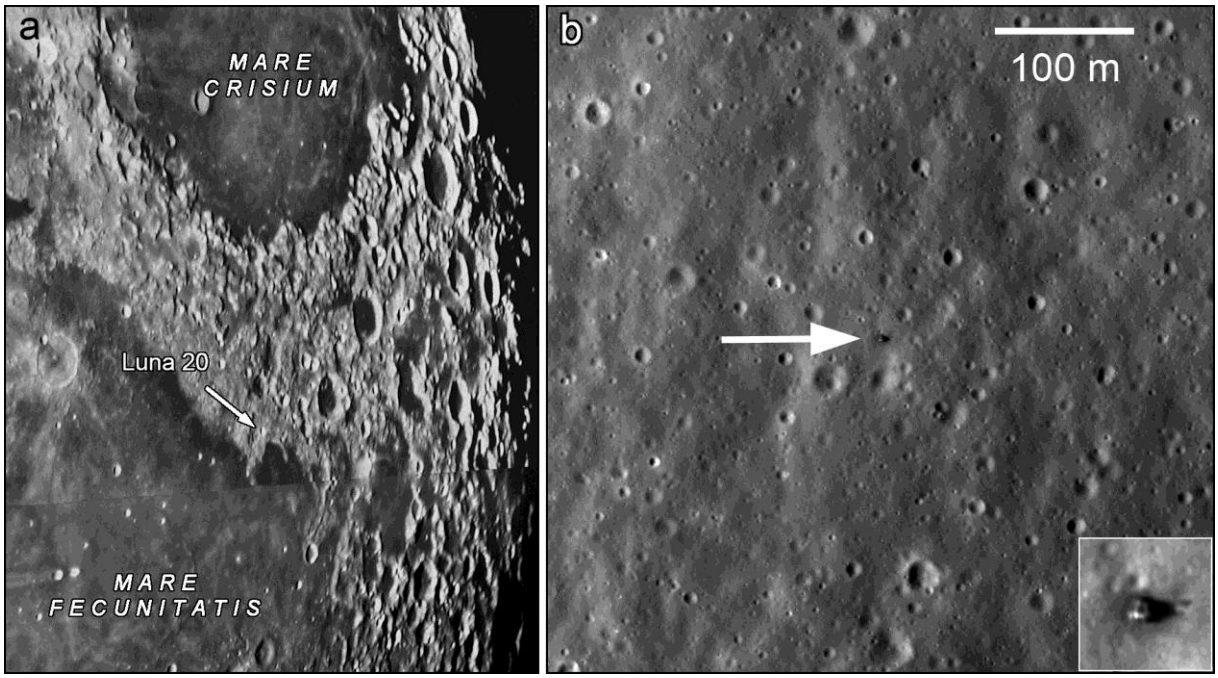

Figure 7. The Luna 20 landing site. a) Mosaic images d2 and e2 from the *Consolidated Lunar Atlas* (http://www.lpi.usra.edu/resources/cla/); b) Part of LROC NAC image M11948286RE, with arrow and inset showing the Luna 20 lander.

It is seen in Figure 7 that the Luna 20 returned samples derived from undulating plains-like terrain covered with numerous craters of meters to tens of meters in diameter. The undulation is due to irregular gentle-sloping grooves trending mostly in the north-south direction and probably being remnants of primary striations within the ejecta from the Crisium basin. The returned sample was a 30-40 cm core of generally fine-grained regolith. Grains with diameters of several hundred microns selected from the bulk sample were used for Ar-Ar age determinations (Cohen et al., 2001).

We acquired 18 determinations of K-Ar age (Figure 2 as well as Figure 5S and Table 5S) from the literature (Cohen et al., 2001 and references therein) for the Luna 20 highland rocks. Among them 7 are impact melt breccias, 3 are no-melt breccias, and 8 are rocks with igneous structures (gabbro, troctolite, anorthite grains). The impact melt breccias show a range of ages from 0.38 to 4.10 Ga with a minor (2 determinations only) peak between 3.85 and 3.90 Ga. The no-melt breccias have ages between 3.84 and 3.90 Ga with a minor peak at ~3.85 Ga while the rocks with igneous structures have ages from 4.02 to 4.36 Ga forming a minor peak between 4.1 and 4.2 Ga. The summary histogram shows two minor peaks at 3.8-3.9 Ga and 4.1-4.2 Ga.

The first age determinations of the Luna 20 samples were made by Podosek et al (1973). These were fragments of highly recrystallized polymict breccias, which showed the same K-Ar age (3.84 ± 0.04 Ga) considered to be a record of a very large impact: either that forming the Imbrium basin or some other nearby basin such as Crisium, Fecunditatis, or Tranquilitatis.

Cadogan and Turner (1977) determined the ages of a sample of metaclastic rock (3.9 ± 0.1 Ga) and a sample consisting of a group of five anorthositic particles (4.3 ± 0.1 Ga). They interpreted the first age as a record of the Crisium basin impact and the second as a record of some other unspecified medium- or large-scale impact.

Huneke and Wasserburg (1979) determined the ages of a fragment of "highland basalt" (they considered that it could be an impact melt) and a fragment of ferroan anorthosite to be ~4.1 and 4.36 Ga respectively, thus confirming the presence of ancient materials at the Luna 20 site. They discussed this in the context of clustering of K-Ar ages of highland rocks at ~3.9 and 4.15 Ga considered by Maurer et al. (1978) and concluded that the age clusters could represent two large impacts or two episodes of intensive cratering by large bodies, but without identifying specific basins which might have been formed by them.

Swindle et al. (1991) determined Ar-Ar ages of 6 samples of impact melts and analyzed their chemical compositions. Two of the six samples, A and E, have exceptionally young ages, 0.52 and 0.38 Ga, respectively, and therefore must represent crater- rather than basin-forming impacts. Two samples, C and D, are compositionally close to the Apollo 17 samples, interpreted by Spudis and Ryder (1981) as Serenitatis impact melts. Their ages are 3.879 ± 0.031 and 3.75 ± 0.11 Ga. The common age of this pair of samples is considered by Swindle et al. (1991) to be 3.85 ± 0.02 Ga and they consider them to represent the Serenitatis impact. Sample F is compositionally distinct from the local soil and from the melt rocks of the Serenitatis and Nectaris basins. It is 3.895 ± 0.017 Ga old and was considered by the authors to represent the age of the Crisium-forming event. Sample B gives a precise age (4.08 Ga) so Swindle et al. (1991) considered it as definitely older than the Imbrium, Serenitatis and Nectaris impacts and probably representing the melt of a large crater formed on typical highlands in pre-Nectarian time.

Cohen et al. (2001) studied 6 samples with igneous structures: two troctolites, two gabbro and two anorthite grains, having Ar-Ar ages from 4.02 to 4.27 Ga. They are considered to record not impacts but magmatic events representing phases of evolution of the Mg-suite of plutonic rocks.

In summary, the K-Ar studied samples from Luna 20 represent two types of materials: 1) impact melts and breccias, and 2) rocks with igneous structures. The former show a variety of ages from ~3.7 to ~4.1 Ga, considered by different workers as records of the Crisium, Imbrium, Serenitatis, Fecunditatis, Tranquilitatis or other unspecified basin(s). The peak of this age subsample occurs at ~3.9 Ga that was considered for the Apollo sites' analyses as the age of Imbrium impact, but keeping in mind that – based on crater counts – the Crisium basin is considered relatively young (younger than Nectaris and Serenitatis according to Fassett et al., 2012) this peak could be due to the Crisium impact event. The rocks of the second type having K-Ar ages from 4.02 to 4.27 Ga are considered to represent events of Mg-suite plutonic magmatism, but one could also suspect that these record an age reset produced by Crisium or other impact events. On the whole, the small quantity of Luna 20 samples in combination with high variability of the measured values make these conclusions very tentative.

3.6. Summary of Apollo-Luna K-Ar age determination

In the above sections we have considered in all 269 K-Ar age values taken from the literature: 117 values for impact melt breccias, 94 for no-melt breccias and 58 for rocks with igneous structures. For the first two lithologic types the connection with large-scale impact events is rather obvious. For the rocks with igneous structures the determined ages, in principle, could record either the time of their formation (crystallization) and/or the time of K-Ar clock resets by subsequent impacts. Keeping in mind that at all sites, the samples were picked up from the regolith or from boulders which are also part of the regolith, and that the bedrock in the lunar highlands is not a real bedrock but different components of impact-produced megaregolith, it may be suggested that the K-Ar ages of the highland rock samples with igneous structures should preferably record not the ages of their magmatic crystallization but impact-induced K-Ar clock resets. To evaluate this suggestion we have checked which, among the 58 samples of such rocks, have also been dated by other techniques using isotope systems (Rb-Sr and Sm-Nd) that are more resistant to the impact induced resets. Among the 58, 9 have been dated this way (Table 3).

Table 3. K-Ar, Rb-Sr and Sm-Nd ages of lunar highland rocks with igneous structures

Sample	Rock type	Site	K-Ar age, Ga	Ref	Rb-Sr age, Ga	Ref	Sm-Nd age, Ga	Ref.
14053	Dolerite	A14	3.85±0.04	1	3.96±0.04	2	-	

15455	Norite	A15	3.85±0.04	3	4.59±0.13	4	-	
60025	Anorthosite	A16	4.11±0.06	5	-		4.36±0.002	6
62236	Anorthosite	A16	3.93±0.04	7	-		4.46±0.04	7
68415	Anorthositic gabbro	A16	3.78±0.06	5	3.84±0.01	2	3.95±0.05	8
72415	Dunite	A17	3.86±0.1	9	4.55±0.01	10	-	
76535	Troctolite	A17	4.25±0.02	11	-		4.33±0.06	12
77215	Norite	A17	3.98±0.03	13	4.42±0.04	14	4.37±0.07	14

Literature sources: 1- Eugster et al., 1984; 2- Papanastassiou & Waserburg; 3- Alexander and Kahl, 1974; 4- Shikh et al., 1993; 5- Schaeffer & Husain, 1974; 6- Borg et al., 2011; 7- Borg et al. 1888; 8- Terra et al. 1973; 9- Dymek et al., 1975; 10- Papanastassiou & Wasserburg, 1975; 11- Park et al., 2015; 12- Premo & Tatsumoto, 1992; 13- Stettler et al., 1978; 14- Nakamura et al., 1976.

We see from the data given in Table 3 that, for all 9 considered samples, the K-Ar age values are lower than the ages determined by the Rb-Sr or Sm-Nd techniques. This suggests that, for these 9 cases and thus probably for the remaining 49 age values of rocks with igneous structures, the Ar-Ar technique recorded the time of an impact-induced clock reset. Thus, they may reasonably be considered in our analysis similarly to the impact-melt and no-melt breccias.

Such an approach shows a prominent peak for the K-Ar age histograms (Figure 2) at ~3.9 Ga over all the considered Apollo sites, which coincides with the time of formation of the Imbrium basin. This peak is the only significant feature on the Apollo 14 and Apollo 15 histograms. This is consistent with the geological position of these two sites within the domain of relatively close ejecta from this basin (Fra Mauro Formation and Montes Apenninus). On the Apollo 16 and Apollo 17 histograms to the right of this peak, towards higher age values, we also see secondary peaks and shoulders. The summary histogram for the Apollo 16 site shows, in addition to the prominent peak at 3.85-3.95 Ga, a shoulder at 3.95 to 4.10 Ga and a minor peak at 4.20-4.25 Ga. The dominant peak seems to represent the material of Cayley Formation considered to be distant ejecta from the Imbrium basin with some admixture of local materials, while the higher age values represent the material of Descartes Formation which is probably dominated by the ejecta of the Nectaris basin. The summary histogram for the Apollo 17 site shows, in addition to the prominent peak at 3.85-3.95 Ga, a notable peak at 4.1-4.2 Ga. The dominant peak seems again to represent the

influence of distant ejecta from Imbrium basin, while the higher age values were suggested to represent the ejecta of the Serenitatis basin.

For a more sophisticated analysis of the collected set of the age values we constructed relative probability plots (some researchers, e.g. Culler et al. (2000), call them ideograms). This technique has been commonly applied for geochronological measurements, and may be understood by analogy with a histogram. However, whereas a histogram requires the choice of a bin-width, and represents each measurement with a single value, a relative probability plot represents each measurement by a probability density function (PDF) – here we use Gaussian distributions – with the 'width' being an intrinsic part of that function, encoded in the standard deviation. The individual PDFs are summed together to produce a summary curve, the magnitude of the sum representing the relative likelihood of the x-value – here, age – having the given value among the samples. The advantage of this treatment is that the uncertainties on individual measurements are neither smoothed nor exaggerated by the choice of binning: you see the spread of the data as it really is.

Below we consider relative probability plots for the Apollo 14 through Apollo 17 and Luna 20 highland rocks and conclude with a consideration of such plots representing all considered Apollo-Luna highland rocks and their lithological varieties: impact melt breccias, no-melt breccias and rocks with igneous structures (Figure 8).

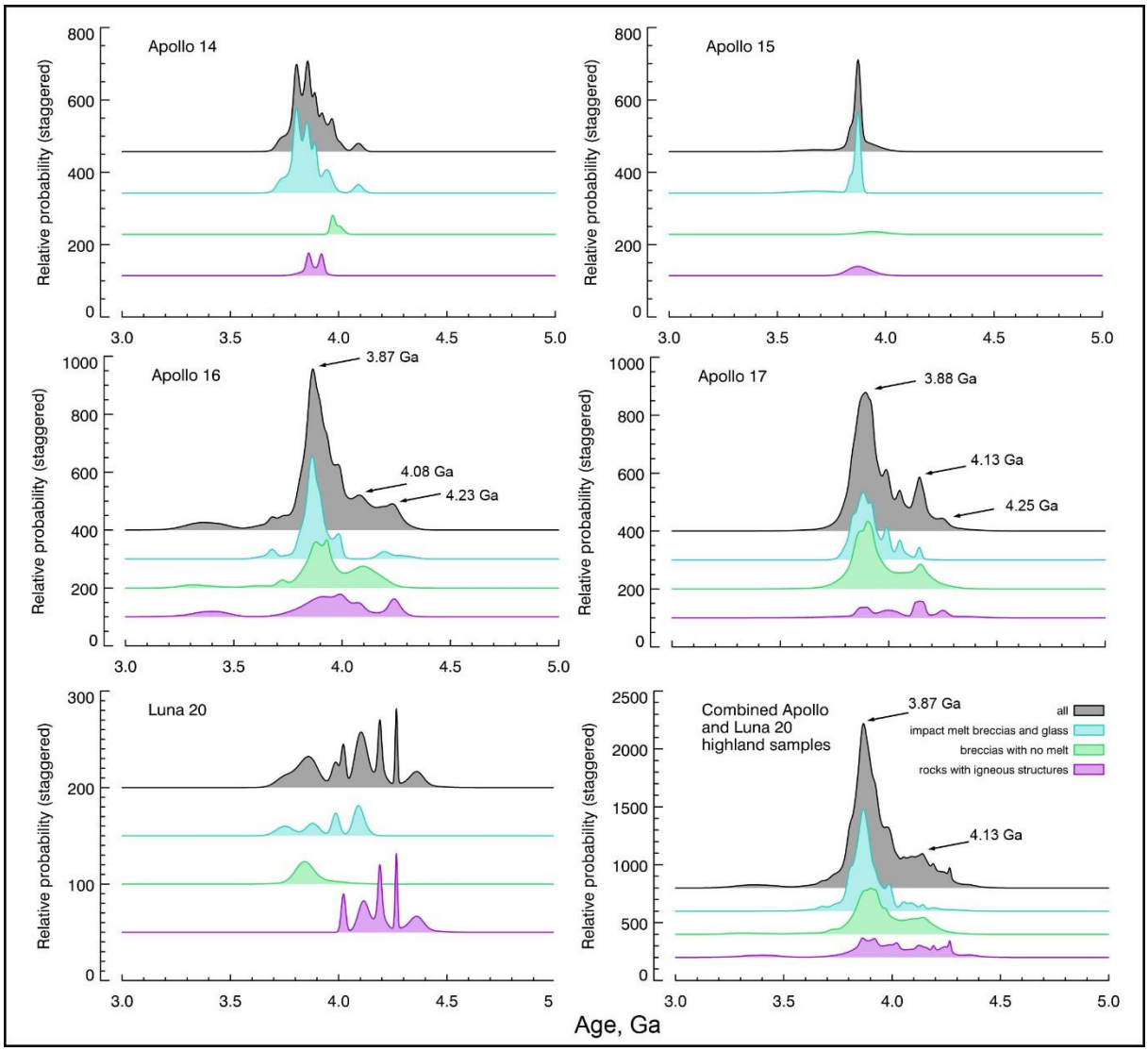

Figure 8. Relative probability plots for the highland rock ages (all and subdivided by lithologies) for the Apollo-Luna sites and the aggregated totals.

Apollo 14. It is seen in Figure 8 that relative probability plots for Apollo 14 melt breccias presenting data for 25 age determination shows a prominent bulge centered at ~3.85 Ga, complicated by four secondary peaks at 3.80, 3.85, 3.89 and 3.95 Ga and one additional peak at 4.10 Ga. Keeping in mind the relatively small number of age determinations these secondary peaks may be within the statistical noise and the meaningful value is probably the center of the bulge (~3.85 Ga). The relative probability plot for no-melt breccias (only 2 age determinations) shows a minor peak at 3.87 Ga, and that for rocks with igneous structures (4 age determinations) shows two minor peaks at 3.87 and 3.92 Ga. The plot for the total set of Apollo 14 highland rocks (31 age determinations) is understandably mainly determined by contribution of the data for the melt breccias. These results generally agree with what was

concluded above for the Apollo 14 highland rocks through consideration of traditional histograms: the formation of Imbrium basin seems to occur at ~3.85 Ga.

Apollo 15. It is seen in Figure 8 that the relative probability plot for Apollo 15 melt breccias presenting data for 8 age determinations shows a prominent peak at 3.87 Ga. The plot for no-melt breccias (only one age determination) shows a minor low bulge centered at ~3.95 Ga. And the plot for rocks with igneous structures (3 age determinations) shows a minor bulge centered at 3.87 Ga. The relative probability plot for the total set of Apollo 15 highland rocks (31 age determinations) is essentially determined by the contribution of the data for the melt breccias. Compared to the traditional histogram consideration above, these results allow a more precise estimate of the peak position (3.87 vs. ~3.9 Ga). According to these data, the formation of the Imbrium basin probably occurred at 3.87 Ga.

Apollo 16. We see from Figure 8 that the relative probability plots for Apollo 16 melt breccias, presenting data for 41 age determinations, show a prominent peak at 3.87 Ga. Three additional minor peaks are observed: at 3.67, 3.98 and 4.20 Ga. The plot for no-melt breccias (also 41 age determinations) shows a slightly broader peak centered at ~3.9 Ga with two small summit promontories at 3.88 and 3.92 Ga and a rather broad but prominent peak centered at 4.10 Ga. The plot for rocks with igneous structures (30 age determinations) shows a prominent bulge extending from 3.8 to 4.1 Ga with an additional smaller peak at 4.23 Ga. The plot for the total set of Apollo 16 highland rocks (112 age determinations) combines the features of the separate lithologies' plots and shows a prominent peak at 3.87 Ga, a shoulder close to 4.0, a smaller peak at 4.08, and another smaller peak at 4.23 Ga. Compared to the consideration of traditional histograms these results allow a more precise estimate of the major peak position (3.87 vs. 3.85–3.95 Ga), confirm a shoulder close to 4.0 Ga, show a secondary but noticeable peak at 4.08 Ga and allow more a precise estimate of the position of the "oldest" peak (4.23 v.s. 4.20–4.25 Ga). Together with what was said in section 2.4 we may conclude that the major peak (3.87 Ga) probably records the formation of the Imbrium basin, the 4.08 Ga peak records the formation of the Nectaris basin, and the 4.23 Ga peak may record the formation of an even older basin.

Apollo 17. The relative probability plots for Apollo 17 melt breccias (Figure 8) presenting data for 36 age determinations show a prominent peak at 3.88 Ga. In the left part of the peak there is a small shoulder at 3.82–3.85 Ga and in the right part there is a small promontory at 3.92 Ga. Towards larger values there are three smaller but clear peaks: at 3.98, 4.05 and 4.13 Ga. The plot for no-melt breccias (47 age determinations) shows a peak centered at 3.9 Ga with a shoulder at 3.86–3.88 Ga and towards the higher values a shoulder

ended with a peak at 4.13 Ga. The plot for rocks with igneous structures (13 age determinations) shows four low peaks centered at 3.88, 4.00, 4.13, and 4.25 Ga. The plot for the total set of the Apollo 17 highland rocks (96 age determinations) combines the features for different lithologies and shows a major prominent peak at 3.88 Ga and four smaller peaks at 3.98, 4.05, 4.13 and 4.25 Ga. Compared to the consideration of traditional histograms these results allow a more precise estimate of the major peak position (3.88 vs. 3.85–3.95 Ga) and split the shoulder with peak at 4.1–4.2 Ga into peaks at 4.05, 4.13 and 4.25 Ga. Together with what was said in part 3.4 we may conclude that the major peak 3.88 Ga) probably records the formation of Imbrium basin, the 4.13 Ga peak records the formation of Serenitatis basin, and the 4.25 Ga peak records the formation of an even older basin, possibly the same one discussed in the above consideration of the Apollo 16 rocks.

Luna 20. We see from Figure 8 that the relative probability plots for Luna 20 melt breccias, presenting data for only 7 age determinations, show four understandably small peaks at 3.75, 3.88, 3.98 and 4.10 Ga. The plot for no-melt breccias (only 3 age determinations) shows a peak centered at 3.85 Ga. The plot for rocks with igneous structures (8 age determinations) shows five small peaks centered at 4.02, 4.12, 4.27 and 4.35 Ga. The plot for the total set of Luna 20 highland rocks (18 age determinations) combines the features of the plots for the different lithologies and shows six smaller peaks at 3.87, 4.02 with a minor promontory at 3.99, and peaks at 4.10, 4.19, 4.27 and 4.35 Ga. Compared consideration of traditional histograms these results do not provide any additional reliable information. The multi-peak shape of three of four considered relative probability plots for Luna 20 is due to the small number of age determinations combined with a rather broad range of measured ages.

All Apollo-Luna highland rocks. The relative probability plot for impact-melt breccias of all sites (Figure 8) shows a major peak corresponding to the age 3.87 Ga. The plot for no-melt breccias shows a major peak at 3.90 Ga that seems statistically not different from 3.87 Ga. The plot for rocks with igneous structures shows several peaks from 3.87 Ga to 4.27 Ga. The combined plot for the set of all considered Apollo-Luna highland rocks shows the major peak corresponding to the age 3.87 Ga, which as discussed before, probably records the formation of Imbrium basin. In addition to the 3.87–3.90 Ga peak there are shoulders and secondary peaks which are the signatures of features seen in the plots for the separate sampling sites. Compared to the consideration of traditional histograms, these results refine the estimate for the major peak from 3.9 to 3.87 Ga. Secondary peaks which were well expressed in the Apollo 16 and 17 plots and linked above with the formation of Nectaris,

Serenitatis and some older basin, are less prominent or even not discernible in the summary plot.

In summary, the use of relative probability plots allowed us to determine the age distribution peaks which we link with several major basin-forming events more precisely: finally, Imbrium at 3.87 Ga, Nectaris at 4.08 Ga, Serenitatis at 4.14 Ga, and one more event at 4.23 Ga. When the number of considered age values is small (Apollo 14, 15, Luna 20) this technique does not yield any further benefit.

3.7. Highland rocks among lunar meteorites

Lunar meteorites are a significant source of lunar highland rocks and provide another route to determine their ages. We have compiled results of K-Ar dating of clasts from 23 lunar meteorites:

1) Alan Hills (AH) 81005, anorthositic regolith breccia. The dated subsample showed an age of 4.300 ± 0.900 Ga (Eugster et al., 1986).

2) Dar al Gani (DaG) 262, anorthositic regolith breccia. Three impact melt clasts were dated: from 2.43 ± 0.17 to 4.12 ± 0.47 Ga (Cohen et al., 2005) and 2 feldspatic fragments: ~1.96 and ~2.89 Ga (Fernandes et al., 2000)

3) Dar al Gani (DaG) 400, anorthositic regolith breccia. 14 impact melt clasts: from 2.56 ± 0.35 to 3.41 ± 0.09 Ga (Cohen et al., 2000, 2005).

4) Dhofar 025, anorthositic regolith breccia. One feldspatic clast: 3.31 ± 0.24 Ga (Fernandes et al., 2004) and 10 impact melt clasts: from 0.56 ± 0.02 to 4.20 ± 1.92 Ga (Cohen et al., 2002).

5) Dhofar 026, anorthositic granulitic breccia. Three impact melt clasts: from 0.57 ± 0.01 to 2.16 ± 0.21 Ga (Cohen et al., 2002).

6) Dhofar 280, anorthositic fragmental breccia. Four clasts: from 2.33 ± 0.41 to 3.72 ± 0.32 Ga (Cohen et al., 2008).

7) Dhofar 303, anorthositic impact melt breccia. One clast of plagioclase: 4.19 ± 0.05, Ga and 6 impact melt clasts: from 2.44 ± 0.03 to 4.47 ± 0.27 Ga (Fernandes et al., 2004).

8) Dhofar 309, anorthositic impact melt breccias. 3.9 ± 0.1 Ga (Korochantseva et al., 2016)

9) Dhofar 489, crystalline matrix anorthositic breccia. One feldspathic clast: 4.23 ± 0.03 Ga (Takeda et al., 2006).

10) Dhofar 730, anorthositic impact melt breccias. 3.0 ± 0.1 Ga (Korochantseva et al., 2016)

11) Dhofar 910 (paired with Dhofar 280), anorthositic fragmental breccia. Four impact melt clasts: from 1.77 ± 0.11 to 3.67 ± 0.15 Ga (Cohen, 2008).

12) Dhofar 911 (paired with Dhofar 303), anorthositic fragmental breccia. One feldspathic clast: 3.50 ± 0.4 Ga and 2 impact melt clasts: 2.70 ± 0.2 and 3.72 ± 0.11 Ga (Cohen, 2008).

13) Dhofar 1435, feldspathic impact melt breccia. Matrix and brown clast: 3.93 ± 0.11 and 3.93 ± 0.16 Ga respectively (Korotchantseva et al., 2009; Korotchantseva, 2011, personal communication)

14) Kalahari, anorthositic regolith breccia. One clast of microporphirite: 2.05 ± 0.04 Ga (Cohen, 2008).

15) MacAlpine Hills (MAC) 88105, anorthositic regolith breccia. Ten impact melt clasts: from 2.47 ± 1.5 to 4.07 ± 0.04 Ga (Bogard et al., 2000; Cohen et al., 2000, 2005).

16) Miller Range (MIL), 090034/090036/090070, anorthositic regolith breccia. Three samples: from 2.62 ± 0.17 to 3.80 ± 0.12 Ga (Park et al., 2013).

17) Northwest Africa (NWA) 482, anorthositic impact melt breccia. Three impact melt clasts: from 2.4 ± 0.02 to 3.75 ± 0.03 Ga (Dauber et al, 2002).

18) Northwest Africa NWA 4472, polymictic regolith breccia. One impact melt clast: from 0.6 ± 0.2 Ga, 1 granulite clast: 2.18 ± 0.05 Ga, and 1 granophyre clast 1.67 ± 0.08 Ga (Joy et al, 2011).

19) Northwest Africa NWA 4881, and paired 3163 and 4883, granulite breccia. 3.4± 0.1 Ga (McLeod et al., 2016).

20) Queen Alexandra Range (Que) 93069, anorthositic regolith breccia. Five impact melt clasts: from 1.84 ± 2.49 to 4.04 ± 0.1 Ga (Cohen et al., 2005).

21) Sayh al Uhaimir (SaU), basalt-bearing anorthositic regolith breccia. Six impact melt clasts: from 1.3 ± 0.02 to 1.66 ± 0.01 Ga (Cohen, 2008) and 1 felspar concentrate: 2.79 ± 0.11 Ga

22) Yamato 791191, anorthositic regolith breccia. One plagioclase rich clast: 4.07 ± 0.09 Ga (Kaneoka and Takaoka, 1986).

23) Yamato 86032, fragmental feldspathic breccia. Two impact melt clasts: 3.80 ± 0.1Ga, and 4 non-melt clasts: from 4.10 ± 0.02 to 4.39 ± 0.06 Ga (Bogard et al., 2000; Nyquist et al., 2006).

So, in total, we considered the K-Ar age values determined in 94 clasts from 23 meteorites, which include two pairs (Dho 280 and 910 and Dho 303 and 911) and thus should represent 21 localities on the Moon. Of these, 73 clasts were impact melt breccias, 13 were no-melt breccias, and 8 were rocks with igneous structures. The distribution of the meteoritic highland rock age values is shown as discrete histograms in Figure 9 and as relative

probability plots in Figure 10. The age values combined with other information on the considered samples are given in Table 6S in the Supplementary materials.

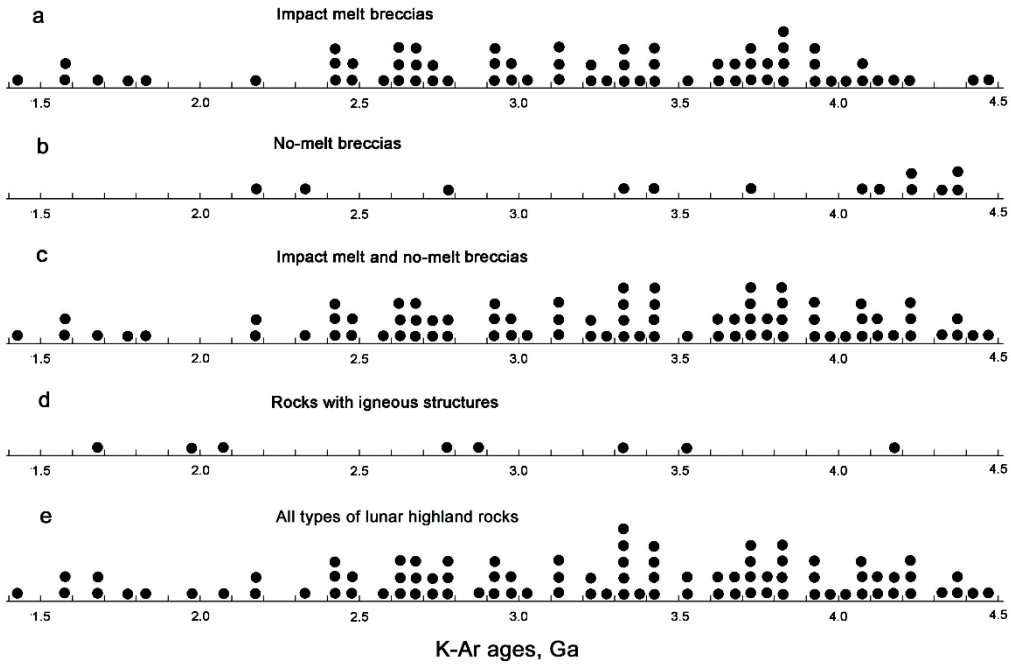

Figure 9. Histograms of K-Ar ages of lunar meteorites: a) impact melt breccias, b) no-melt breccias, c) impact melt and no-melt breccias, d) rocks with igneous structures, e) all types of lunar highland rocks. There are eight age values lower than 1.4 Ga which are not shown in this figure.

It is seen from Figure 9 that the majority of considered K-Ar ages results from the impact melt breccias (Figure 9a), so that their distribution is close to that of the summary histogram for all types of lunar meteorite highland rocks (Figure 9e). No-melt breccias (Figure 9b) show a possible concentration of ages between 4.0 and 4.4 Ga while the rocks with igneous structures (Figure 9d) show no notable feature. Both represent relatively small fractions of total of considered age values so their role in the character of the summary histogram (Figure 9e) is not significant. The summary histogram shows that the K-Ar age distribution of the considered meteoritic highland rocks has no prominent peak around 3.9 Ga as is typical for the Apollo 14–17 highland rocks. Instead we see a broad and low concentration between 2.4 and 4.4 Ga with no significantly larger peaks.

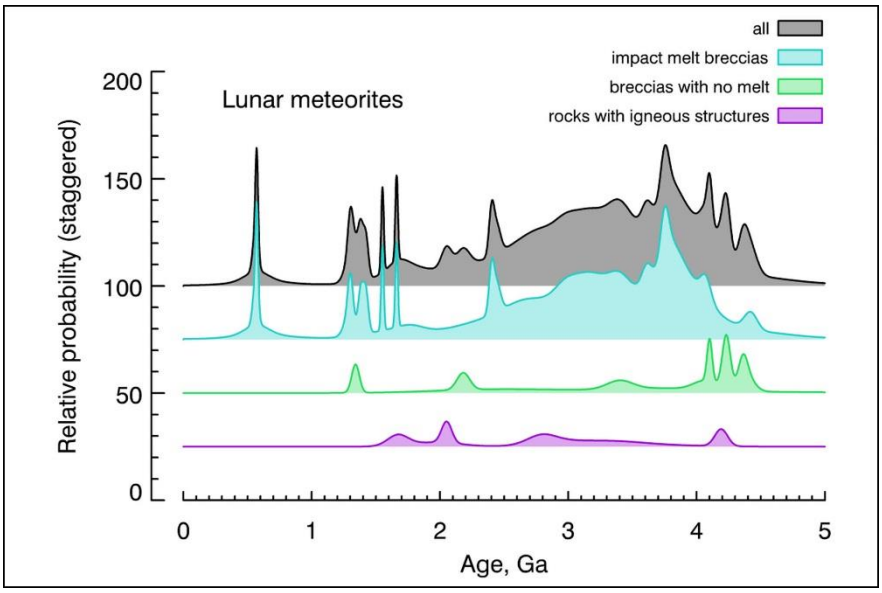

Figure 10. Relative probability plots of K-Ar age distribution for all considered meteoritic highland rocks and their lithological varieties: impact melt breccias, no-melt breccias and rocks with igneous structures.

Figure 10 shows that both the impact melt breccias and all the considered meteoritic highland rocks together show an asymmetric bulge with a broad maximum between 3 and 4 Ga. The bulge gradually slopes down to ~4.5 Ga and more gently slopes down to ~1 Ga. The bulge is complicated by several narrow peaks, which, as it was noted in consideration of histograms of Figure 9, are produced by individual precise measurements. No predominant peak around 3.9 Ga, as is typical for the Apollo 14–17 highland rocks' histograms and relative probability plots, is seen here.

The distribution of the K-Ar ages of lunar meteorites was first discussed in the context of the problem of the lunar cataclysm when the number of dated lunar meteorites came to be significant. Cohen et al. (2000) considered results of dating of 31 clasts from 4 meteorites representing lunar highland rocks: DaG 262 (3 clasts), DaG 400 (14 clasts), MAC 88105 (9 clasts) and QUE 93069 (5 clasts). They found that the K-Ar age distribution did not show a prominent peak at ~3.9 Ga, as was found for the Apollo highland rocks samples and then considered as evidence for a lunar cataclysm (e.g., Ryder, 1989, 1990; Stoffler and Ryder, 2001; Taylor et al., 1991).

In the considered group of 31 age values, Cohen et al. (2000) identified 7 so-called individual impact events. They defined these as ages which were sufficiently close to each other as recorded by two or more clasts in a single meteorite. For DaG 262 no individual impact events were found. For DaG 400 they identified three impact events; for MAC 88105

two impact events were identified; and for QUE 93069 two impact events were also identified. Despite the rather wide time interval (2.76–3.92 Ga) of the identified impact events, Cohen et al. (2000) stated that the results supported the hypothesis of a terminal cataclysm, considering "the lack of impact melt older than 3.92 Ga" (their page 1154) as the major argument.

In later work these authors considered a larger number of dated clasts: 42 compared to the previous 31 (Cohen et al., 2005). The ages discussed in this paper were "isochron- or proxy-corrected ages" (their Table 5). In this work they show about 6 impact events slightly different from those described in Cohen et al. (2000). As in the previous work, they state: "No meteorite impact melts have ages more than 1σ older than 4.0 Ga" (Cohen et al., 2005). This time, however, their general conclusion was significantly softened: "This observation is consistent with, but does not require, a lunar cataclysm".

In our sample of 94 K-Ar ages, representing 21 localities on the Moon from which the meteorites were ejected, 16 ages are older than 4 Ga (from 4.01 ± 0.2 to 4.47 ± 0.27 Ga) and among them 12 ages are more than 1σ older than the assumed 3.9 Ga cataclysm age. Of these 12 ages, six were determined for the feldspar clasts and the remaining six for impact melt clasts. Thus, meteorite impact melts with K-Ar ages more than 1σ older than the assumed age of lunar cataclysm are described in publications, contradicting the findings of Cohen et al (2002, 2005). Bearing in mind that the feldspar clasts may be fragments of well-crystallized impact melts, our assertion of the existence of 'pre-cataclysm' impact melts is even more solid.

Our summary plot of the K-Ar age frequency distribution, like the results of Cohen et al. (2000, 2005), shows no peak around 3.9 Ga ago as should be expected if the lunar cataclysm did occur. Moreover, there is no noticeable increase in the frequency of the impact melt ages older than 3.9 Ga although there is no doubt that between 4.5 and 3.9 Ga ago there was heavy bombardment. Under debate is only the question of whether, during that time period, there was a gradual decline in cratering intensity or there was a prominent intensity spike around 3.9 Ga ago.

These features were noticed and discussed by Hartmann (2003), Hartmann et al. (2007) and Chapman et al. (2007). These authors also noticed the absence of the ~3.9 Ga cataclysm peak and the absence of an increase in the frequency of the impact reset ages older than 3.9 Ga in chondrites and HED achondrites (e.g. Bogard, 1995). This is an important observation because early intense bombardment and the lunar terminal cataclysm (if the latter occurred) are broadly accepted to be a general characteristic of the inner Solar System (e.g.,

Murray et al., 1975; Mutch et al., 1976; Wood and Head 1976; Fassett and Minton, 2013; Marchi et al., 2013). Later work by Bogard and Harrison (2003) provided more details on the distribution of impact reset ages of eucrites. Based on their work, Figure 11 shows that as in the earlier set of data (Bogard, 1995), the ~3.9 Ga cataclysm peak is absent.

A feature in this updated data set not observed earlier is the appearance of a prominent peak at 4.50 ± 0.05 Ga, which authors related to the formation of the 460-km Rheasilvia Crater on Vesta, first seen with the Hubble telescope (Thomas et al., 1997). However, the analysis of crater counts in images acquired by the Dawn mission (Schmedemann et al., 2014) showed that this giant crater has a formation age of 3.5 ± 0.1 Ga and thus is unlikely to be responsible for the peak at 4.50 Ga. The later summary of Bogard (2011) involving additional Ar-Ar age measurements of eucrites shows a relative probability plot (his Figure 8) similar to what is shown in our Figure 11 with no peak at 3.9 Ga.

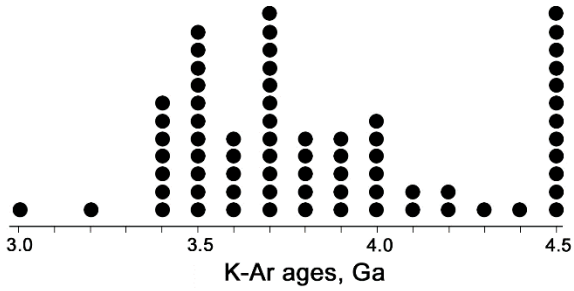

Figure 11. Histogram of K-Ar impact reset ages of eucrites adopted from Figure 11 of Bogard and Garrison (2003).

Hartmann (2003) and Hartmann et al. (2007) suggest that the observed frequency distribution of K-Ar ages of lunar meteorites is due to later cratering which, even being of lower intensity, destroys the earlier formed impact melt/glass records causing a bias towards younger ages. Chapman et al. (2007) disagree with details of the Hartmann (2003) and Hartmann et al. (2007) explanation of the older age deficit, but agree that the mentioned bias towards the younger ages does exist. They state that to resolve the mechanism of the bias, a "quantitative comparison of the statistics of ages … with realistic modeling of basin formation, megaregolith evolution and surficial regolith processing of ancient materials" is required. In the next section of this work, we develop a model to consider the mixing of basin melt into the megaregolith by subsequent impacts, with the goal of understanding how the abundance of basin melt should evolve with respect to the near-surface, which is the source of

the collected samples and, most probably, the ejected meteorites. We then compare our age summaries with the model predictions.

4. Evolution of the presence of impact melt at the near-surface of the Moon

4.1 Introduction

The purpose of the modelling in this section is to attempt to understand the cumulative effect of *impact gardening* – the process by which surface material is redistributed, mixed, and remelted by impact events – on the presence of impact melt of different ages at the near-surface of the Moon. We shall use this knowledge to help evaluate the context of the ages measured from actual surface samples.

It is possible to make reasonable estimates of the amount of melt produced by impact events of differing scales, and likewise the depth of excavation and the quantity of unheated material which is redistributed at the surface. However, the cumulative effect of a long sequence of impacts melting, excavating, burying and re-excavating material produces a megaregolith which is complex in its melt distribution with depth. The characteristics of the distribution depend on the size–frequency distribution of craters forming on the surface, commonly called the crater production function. Furthermore, to trace back the presence of melt specifically for the Moon, we also need to have some understanding of the history of its crater formation rate.

4.2 How the model works

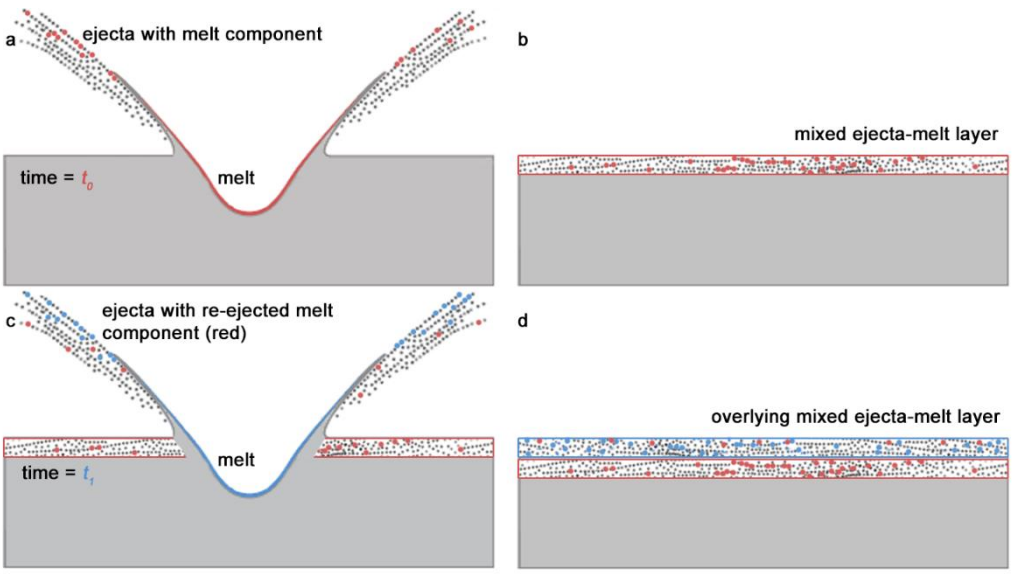

Figure 12. Schematic of the simulations showing a) impact event causing ejection of both unheated (grey) and melted material (red), b) the deposition of a mixed layer of unheated ejecta and melt, c) a subsequent impact event, ejecting material from both the previous layer (grey/red) and beneath, melting a fraction of both (blue), and d) depositing a new layer containing both new melt and a component of re-excavated melt from the previous event.

The essence of the model, illustrated in Figure 12, is the following:

1. An initial volume, with a surface area equivalent to that of the Moon is denoted with a nominal starting age of T_0 (we take 4.5 Ga), and a minimum crater size for the simulation is chosen, D_{min}.

Impact timing

2. From the lunar chronology function (Neukum, 1983), an impact rate is found for the current model time, T, which corresponds to craters of 1 km in diameter. By means of the crater production function, the equivalent rate for craters of size D_{min} is found.
3. The rate gives the average time to the next impact event producing a crater larger than D_{min}. With a Monte Carlo approach, we can use a Poisson function to find realistically distributed time intervals, although for the large number of events being simulated, it can be sufficient to employ an averaged interval.

Crater size

4. The diameter of the crater formed is generated using the Monte Carlo method in such a way that the size–frequency distribution statistically conforms to the portion of the production function larger than D_{min} (Michael et al., 2016). The largest crater produced this way is limited by the range of validity of the production function: in the case of the Neukum (1983) function, $D_{\mathrm{max}} = 300$ km. The transient cavity diameter is estimated as $D_{\mathrm{tc}} = (D_{\mathrm{f}}\, {D_{\mathrm{c}}}^{0.13}/1.17)^{1/1.13}$ (McKinnon et al., 1997), where D_{f} is the measured final diameter and D_{c} is the simple–complex transition diameter, taken as 19 km (Pike, 1980).

Excavation

5. For each crater produced, the maximum depth of excavation is calculated as $D_{\mathrm{tc}}/10$ (Melosh, 1989). The excavated volume has a torus-like shape, which we estimate to occupy about 1/3 of the volume of a disc of this thickness.

Production of melt/heated material

6. A portion of the excavated volume is considered to have been melted (or alternatively, heated above the point required to reset the K-Ar clock): $\mathrm{r_{melt}} = \mathrm{cD_{tc}^{d}/V_{tc}}$, where D_{tc} and $\mathrm{V_{tc}}$ are the diameter and volume of the transient crater, and *c* and *d* for an average density impactor are taken as 1.4×10^{-4} and 3.85, respectively (after Cintala and Grieve (1998)). The melted material is marked in the simulation with the current clock time, T.

Material redistribution

7. The excavated material, together with the new melt, is redistributed evenly over the entire surface of the body. This is a significant simplification, which we justify by the intention to obtain an average picture of the lunar state. Because of the relative frequency of smaller impacts whose ejecta do not travel so far, such an approach should nevertheless provide a reasonable reflection of the amount of ejecta sourced from craters of differing sizes at any point of the surface.

   We know that during ejecta emplacement from impact craters forming on Earth, a large quantity of local substrate material becomes entrained and thoroughly mixed into the continuous ejecta (Hörz et al., 1983). The degree of mixing with substrate material should be a function of the substrate strength, cohesion, and possibly on Earth – the presence of water. We expect low cohesion in the lunar regolith, but the depth of mixing is difficult to estimate. We do not account for this process, but acknowledge it may be significant.

Iteration

8. If the model time has not yet reached the present, $T = 0$, continue from step 2.

Thus, the situation in the model after the first impact is that there is the initial volume of age T_0 covered by a thin layer of ejecta which has a dispersed small fraction of its volume carrying the later age T_1, but the remainder carrying the original age, T_0.

The second impact penetrates the thin layer into the initial volume, and excavates material from both: from the thin layer, a disc of volume $\pi D^2 d/4$ where d is its thickness, and the remainder from the underlying volume. The ejected volume, then, contains a very small fraction of melt from the previous impact. For simplicity, the location of melt formation within the transient crater is not considered, but taken to be a fraction of the entire ejected volume. Most of the new melt will be of material of the original age T_0, but a tiny component will be remelted melt from the previous impact. This tiny component now carries the age of the new impact, T_2, and accounts for a reduction in the total presence of melt of age T_1.

The simulation proceeds in a similar manner, each impact excavating material from previous ejecta layers together with ‘original’ material until the ejecta coverage becomes sufficiently thick that, for certain sizes of crater, the whole of the ejected volume is recycled ejecta: at this point we have reached the stage of so-called impact gardening. However, each impact continues to melt a fraction of every differently-aged component of the material it ejects: larger impacts bringing up material from deeper layers; lesser ones recycling the material nearer the surface.

To ensure that the model conserves the mass in the system, each time a layer is penetrated and its material redistributed, the volume of the layer is diminished accordingly. This is achieved in the model by reducing the thickness of the layer. Again, this simplification can be understood in an average sense: the amount of ejecta from a given impact residing at a given depth is diminished by having holes punched in it. It is not really diminished evenly, but on average, the amount of ejecta you could expect to find from craters of a given diameter at a given depth should be equivalent. The goal, finally, is to produce an average picture of the melt distribution: in age, and with depth. The model is scrupulous in maintaining the quantities of melt/non-melt of different ages; the simplifications made in accounting for the depth of location of the components are, we believe, adequate not to severely distort the general picture.

We note that, for the present, the model makes no account for other endogenic processes, and assumes a homogeneous surface. We make no account, for example, of the influence of the maria or their emplacement processes.

The ejecta layers in the model are each represented by a time-resolved histogram of the components of different ages. As the simulation progresses, the number of layers becomes large, increasing the computational cost of calculating the age composition of material from an excavated crater. To alleviate the problem, the stack of layers is periodically amalgamated into a simpler one, whereby each deeper layer is twice as thick as the one above it, but precisely conserving the composition of the stack. This technique preserves a rather fine resolution of the melt distribution near the surface while maintaining a more averaged distribution at greater depths.

4.3 Results

To make the influence of the various aspects of the model clear, in this section the different components of the simulation are introduced one at a time.

Fixed crater diameter, event resolved model

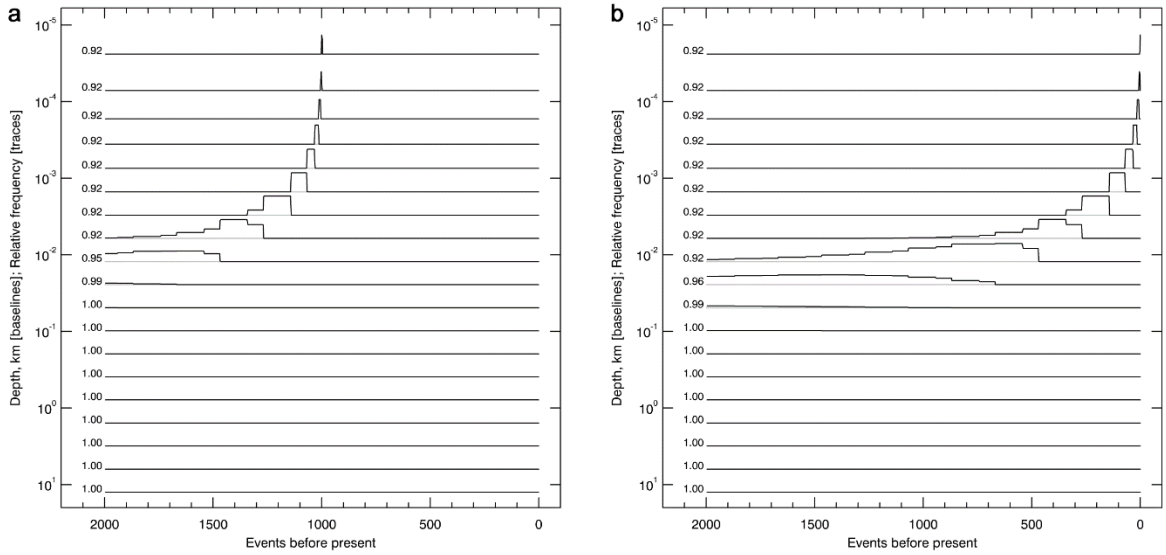

Figure 13. *Fixed crater diameter, event resolved model*. Result of a simulation of 2000 impact events with impactors of constant size, producing craters 30 km in diameter after a) 1000 events and b) 2000 events. Each trace in the plot represents a histogram of the presence of differing melt ages, the baseline of the trace being plotted at the layer's depth below the surface according to the vertical axis scale, with all traces using the same normalisation. The numbers at the left side of each trace show the fraction of material of age τ_0 that has never been melted during the simulation (this fraction is excluded from the histogram, since it would plot much higher). The time scale, in this case, is measured in events: i.e. the age of the melt is specified by the sequential number of the event in which it occurred.

Figure 13 shows the result of a simulation of 2000 impact events with impactors of constant size, producing craters 30 km in diameter. Each trace in the plot represents a histogram of the presence of melt of differing ages, the baseline of the trace being plotted at the layer's depth below the surface according to the vertical axis scale. The age scale, in this case, is measured in events: i.e. the age of the melt is specified by the sequential number of the event in which it occurred. The vertical scale for the individual histograms is not shown, but each trace is plotted with the same scale. The figures at the left end of the traces show the fraction of material of age T_0 that has never been melted during the simulation (this fraction is excluded from the histogram, since it would plot much higher). Figure 13a shows the state of the model after 1000 events, and Figure 13b – after 2000.

The plots can be interpreted as follows: the melt from the most recent impact is most prominent at the surface, in the top trace. With increasing depth, and increasing cumulative thickness of the layers used to construct the figure (doubling between each trace and the next), we see the covered ejecta of previous impacts going back in time. The melt shown here is predominantly primary melt: the 30-km-crater forming impacts excavate material from around 3 km depth, but even at the end of the simulation only around 3% of the top 100 m is available to produce secondary melt (by which we mean melt from a previous event that is re-melted). The stepped nature of the deeper histogram curves is a consequence of the layer amalgamation procedure: in the first amalgamation, groups of fine layers are averaged into progressively larger layers with depth. Later in the simulation, after a sequence of additional fine layers has been deposited on top of this set and a second amalgamation occurs, a formerly thick layer is typically split across the boundary of two layers in the amalgamation: thus we see a portion of the peak move into the layer below.

Realistic crater diameter, event resolved model

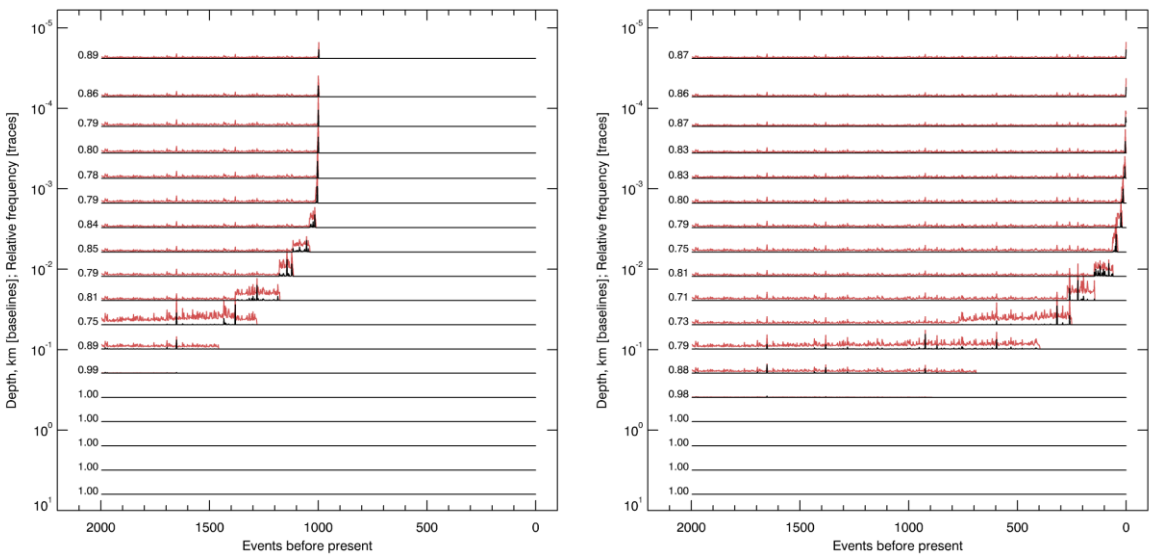

Figure 14. *Realistic crater diameter, event resolved model.* Result of a simulation of 2000 impact events producing craters larger 30 km drawn randomly from the realistic size–frequency distribution described by Neukum (1983) after a) 1000 events and b) 2000 events. Each trace in the plot represents a histogram of the presence of differing melt ages, the baseline of the trace being plotted at the layer's depth below the surface according to the vertical axis scale. The histograms are plotted twice: in black – with all traces using the same normalisation; in red – with exaggerated small values. The numbers at the left side of each trace show the fraction of material of age τ_0 that has never been melted during the simulation

(this fraction is excluded from the histogram, since it would plot much higher). The age scale, in this case, is measured in events: i.e. the age of the melt is specified by the sequential number of the event in which it occurred.

Figure 14 shows the result of a simulation of 2000 impact events drawn from a realistic size–frequency distribution to match the production function seen on the Moon, with a minimum diameter of 30 km. According to the function, around one in ten events will produce a crater larger than 80 km diameter; around one in a hundred will produce a crater larger than 170 km diameter; and about one in 430 will produce a crater of 300 km diameter, the largest in the defined range of the production function. This time, the melt is seen at much greater depths, the difference being that a 30 km crater produces an averaged (as discussed above) global ejecta coverage of about 20 cm depth compared to a 300 km crater, at the other extreme, producing an averaged layer of about 190 m thickness. The histogram data are plotted twice: once in black, using the same normalisation over all the traces; and a second time in blue, where the small values are exaggerated by plotting $y = h^{0.25}$, where h are the normalised histogram values. This makes it easier to see the development of the structure in the simulation results, where otherwise the values would be too small.

It is evident that the near-surface melt is dominated by the most recent impacts, while further back in time, it is the largest impacts which are prominent. It is notable that the larger impacts produce sufficient melt to leave a permanent signature in the upper layers (for example, the impacts occurring around events 1650, 930). Later impacts of lesser scale either penetrate to the original ejecta layer to bring up more of its melt, or recycle the same aged melt nearer the surface. Eventually the melt from these events becomes present at every depth down to its source ejecta layer.

Fixed crater diameter, time-resolved model

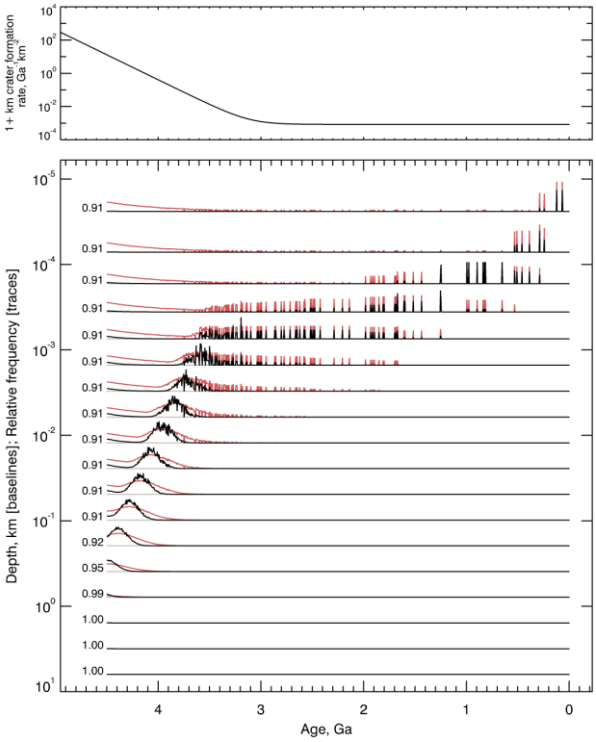

Figure 15. Fixed crater diameter time-resolved model. Result of a simulation using a fixed crater size of 30 km, but this time simulated for a period of 4.5 Ga using a realistic impact rate function, plotted above (Neukum, 1983). The horizontal axis, instead of showing events, indicates the age of the melt. Each trace in the plot represents a histogram of the presence of differing melt ages, the baseline of the trace being plotted at the layer's depth below the surface according to the vertical axis scale. The histograms are plotted twice: in black – with all traces using the same normalisation; in red – with exaggerated small values. The numbers at the left side of each trace show the fraction of material of age τ_0 that has never been melted during the simulation (this fraction is excluded from the histogram, since it would plot much higher). The simulation represents a sequence of about 40,000 events.

Figure 15 shows the result of a simulation using a fixed crater size of 30 km, but this time simulated for a period of 4.5 Ga using a realistic impact rate function (Neukum, 1983). The near-surface, as before, is dominated by the most recent events. The mid-depth traces of the plot have a comb-like appearance because the individual events are resolved. Note that the events are spaced in time with Poisson-distributed intervals. As before, each successive layer is seen to contain about twice as many peaks, consistent with the doubling thickness of the model layers. If this graphic were plotted with an event scale, the doubling would be apparent all the way down to the layer at about 500 m depth (note that the rate function as given yields about 40,000 events). However, using the realistic rate function with a time scale causes the event peaks older than 3 Ga to be increasingly compressed together such that the doubling

appears as a smooth maximum moving back linearly in time. This is the effect of the exponential term in the chronology function:

$$N(1) = 5.44 \times 10^{-14}\,(e^{6.93t} - 1) + 8.38 \times 10^{-4} t$$

which describes the cumulative number of craters larger than 1 km diameter formed per square kilometre over a time period *t* in Ga counted backwards from the present (Neukum, 1983). Additionally, we see a rise in the presence of melt from around 3.5 Ga going back to the beginning of the simulation at 4.5 Ga. This is the contribution of re-excavated melt from the exponentially higher frequency early impacts.

Realistic crater diameter, time-resolved model

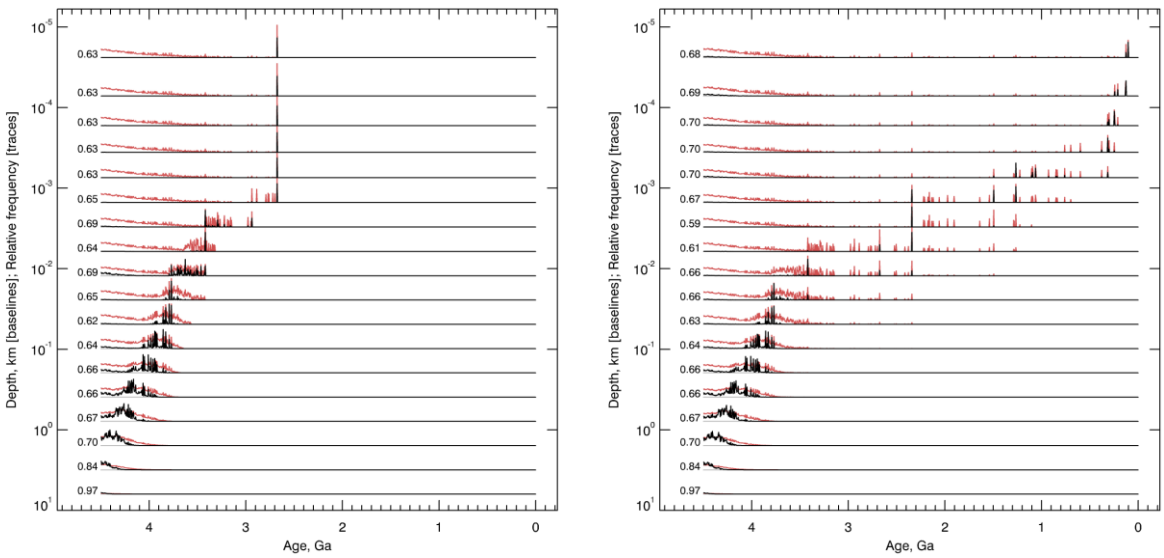

Figure 16. Realistic crater diameter, time-resolved model. Result of a single realisation of the simulation using craters larger 30 km drawn randomly from the realistic size–frequency distribution described by the Neukum (1983) production function over a period of 4.5 Ga using a realistic impact rate function after a) 39201 events (~2.8 Ga before present) and b) 39245 events (last event before *T=0*). The horizontal axis indicates the age of the melt. Each trace in the plot represents a histogram of the presence of differing melt ages, the baseline of the trace being plotted at the layer's depth below the surface according to the vertical axis scale. The histograms are plotted twice: in black – with all traces using the same normalisation; in red – with exaggerated small values. The numbers at the left side of each trace show the fraction of material of age τ_0 that has never been melted during the simulation (this fraction is excluded from the histogram, since it would plot much higher). The

simulation represents a sequence of about 40,000 events (note that ~38,000 of these occur before 4 Ga). Rate function as in Figure 15.

Figure 16 shows a simulation using crater sizes drawn from a realistic size–frequency distribution for a simulated period of 4.5 Ga, using a realistic rate function. As before, by comparison with the fixed diameter simulation, the realistic diameter simulation shows melt present to a greater depth. The general characteristics of the fixed-diameter simulation remain: the descending characteristic of increasingly deeply buried ejecta going back in time; the rise in the presence of melt before 3 Ga, when the impact rate was highest, representing material re-excavated and mixed into all of the upper layers. Also recognisable are the intermittent peaks from the largest impacts which become mixed into all the layers above them. We see the mixing process in Figure 16a where, for example, recent impacts have brought up pre-4 Ga material, seen now on the seventh histogram trace (10 m depth, black line). By the end of the simulation, about 50 events later (Figure 16b), this feature has been dispersed into deeper levels. This small number of events arises because the impact rate over the final 3 Ga is about 100 times lower than at 3.8 Ga and 10 000 times lower than at 4 Ga.

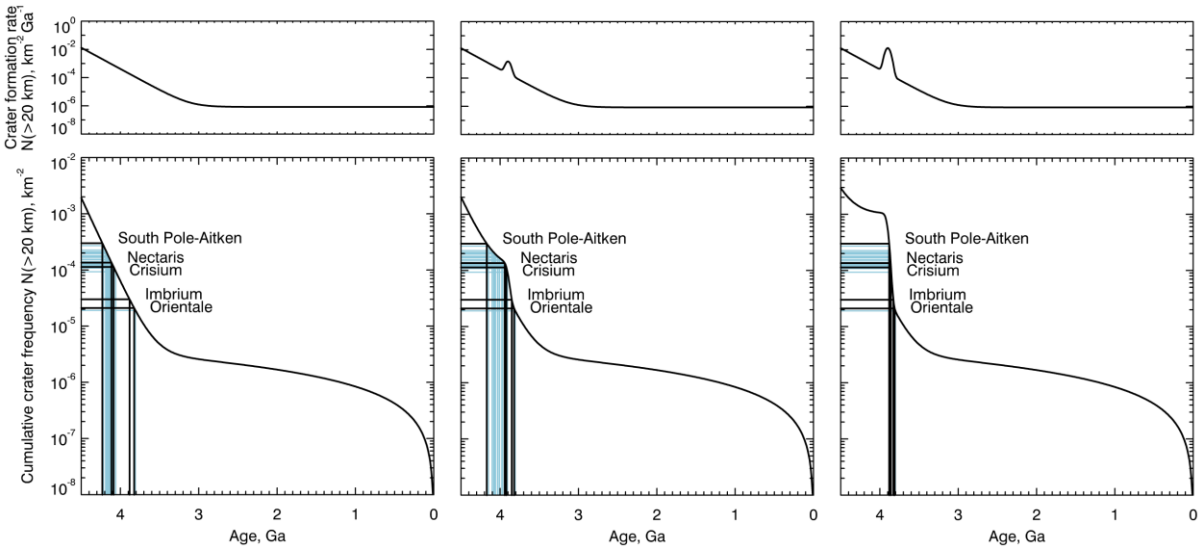

Figure 17. Plausible distribution of time points for basin forming events as predicted from N(20) crater densities measured by Fassett et al. (2012) within a) the Neukum (1983) chronology model (above as rate function; below in cumulative form) b) the same model with the addition of a ‘cataclysmic peak’ into the impact rate function at 3.9 Ga, c) the same model with the addition of an extreme ‘cataclysmic peak’ at 3.9 Ga. The five largest basin events, South Pole – Aitken, Nectaris, Crisium, Imbrium and Orientale are labelled and indicated with black lines; the remaining 22 with blue lines only.

Realistic crater diameter, time-resolved model with basin events

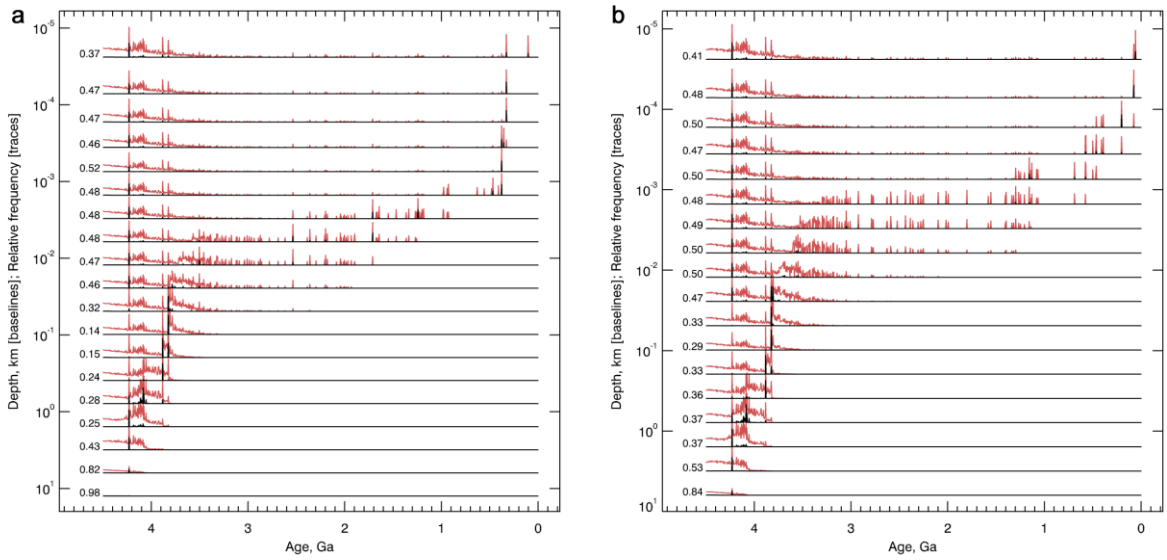

Figure 18. *Realistic crater diameter, time-resolved model with basin events.* Results of two runs (*a*, *b*) of a simulation using craters of random size larger 30 km conforming to the size–frequency distribution described by the Neukum (1983) production function over a period of 4.5 Ga using a realistic impact rate function and incorporating basin-forming events. The horizontal axis indicates the age of the melt. Each trace in the plot represents a histogram of the presence of differing melt ages, the baseline of the trace being plotted at the layer's depth below the surface according to the vertical axis scale. The histograms are plotted twice: in black – with all traces using the same normalisation; in red – with exaggerated small values. The numbers at the left side of each trace show the fraction of material of age τ_0 that has never been melted during the simulation (this fraction is excluded from the histogram, since it would plot much higher). The four prominent peaks present in both runs represent South Pole – Aitken at 4.23 Ga, Crisium at 4.08 Ga, Imbrium at 3.88 Ga and Orientale at 3.82 Ga (modelled timings derived from N(20) values from Fassett et al. (2012)). Rate function as in Figure 15.

Although the lunar basins may be considered the large diameter tail of the crater size–frequency distribution, for the purpose of this model it makes more sense to treat them separately. If we were to extend the crater production function to include basin forming events, a random sampling from it in the manner of this simulation would produce a substantially different Moon on each run. Sometimes there might be two basins of South Pole – Aitken scale; sometimes none. Such Moons might have formed in an equivalent flux of impactors, but would be markedly different from the one we know. For craters, the situation is

different: because of their large number, every run produces a result which is statistically rather similar (nevertheless, there are differences in when the larger impacts occur). Therefore, instead of generating the basin-forming events randomly, in the simulation they occur according to a table of the actual lunar basins. The times for their occurrence are calculated according to the N(20) crater densities measured by Fassett et al. (2012) using the chronology function, modifying the values for SPA and Serenitatis to 300 and 155 per million km^2 respectively to force them into the stratigraphic sequence of their Table 1. We take this approach to generate a plausible spread of time points in lunar history for basin forming events in different impact rate scenarios, but not claiming accurate knowledge of the age of any particular basin (Figure 17).

Figure 18 shows two realisations of the Monte Carlo simulation including basin-forming impacts, based on different random number sequences. First of all, we see that the amount of unmelted material close to the surface (shown by the numbers at the beginning of each trace) is reduced from ~70% in the previous simulations to ~40%. The series of 27 basin-forming events produce together more melt than all the remaining ~40,000 crater-forming events. The histograms show four prominent peaks which are consistent between the two runs: these represent South Pole – Aitken at 4.23 Ga, a cluster of peaks around Crisium at 4.08 Ga, Imbrium at 3.88 Ga and Orientale at 3.82 Ga (we note these ages only for identification of the features in the figure: they are not definitive). The remainder of the traces remain as before, but we see less detail because of the normalisation to the larger basin-forming events.

In the near-surface layer, beginning with the youngest melt, we see two peaks representing the final impact events (100 and 320 Ma) with abundances of 5–7% (Figure 18a). Prior to these we see the traces of several events (e.g. at about 1.7 and 2.5 Ga) which have stronger abundances at around 10 m depth. Then we see the exponential impact rate rising before 3 Ga with prominent peaks for Orientale and Imbrium (3% and 4% surface abundance, respectively). South Pole – Aitken appears as the oldest peak with roughly 20% abundance at the surface. At the end of the simulation—representing the present day—the most common melt at the surface is from the four above-mentioned basin events, along with an admixture from very recent impacts.

Comparing the two runs in Figure 18, we see that the different realisations of the Monte Carlo simulation produce visibly different features in the post-basin period melt structure. This is

mainly determined by when the larger impacts occur: we see larger events at around 2.5 and 1.7 Ga in the first run, and at around 3.05 and 1.2 Ga in the second, in the former instance showing the majority of melt in the 5–10 m depth range with lesser components recycled up to the surface. In all such simulations the general tendency for later impacts to leave traces at the surface is maintained, and should be expected in surface samples.

Cataclysm scenario

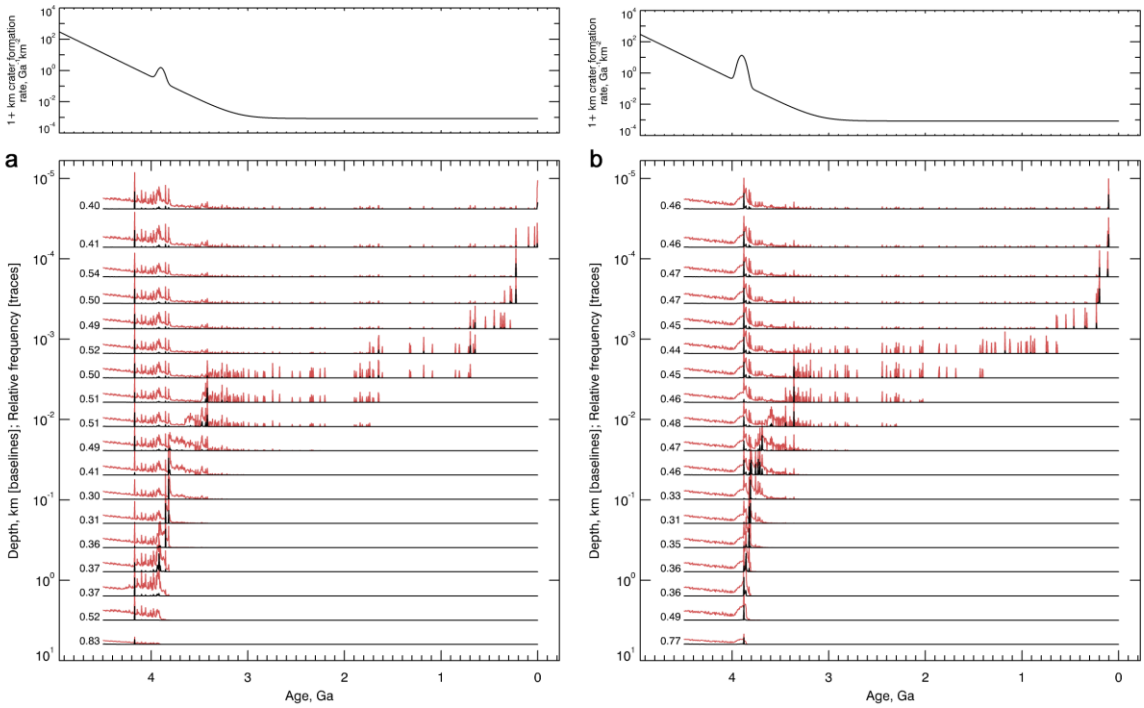

Figure 19. *Cataclysm scenario.* Result of two runs of a simulation using craters of random size larger 30 km conforming to the size–frequency distribution described by the Neukum (1983) production function over a period of 4.5 Ga using a hypothetical impact rate function and incorporating basin-forming events with a cataclysmic peaks (plotted above) of relative magnitudes a) 1 and b) 10. The horizontal axis indicates the age of the melt. Each trace in the plot represents a histogram of the presence of differing melt ages, the baseline of the trace being plotted at the layer's depth below the surface according to the vertical axis scale. The histograms are plotted twice: in black – with all traces using the same normalisation; in red – with exaggerated small values. The numbers at the left side of each trace show the fraction of material of age τ_0 that has never been melted during the simulation (this fraction is excluded from the histogram, since it would plot much higher). The four prominent peaks again represent South Pole – Aitken, Crisium, Imbrium and Orientale, but now they have been either partially or fully compressed into a cataclysmic peak centred on 3.9 Ga.

Figure 19 shows the result of two simulation runs identical to the previous one, but with the addition of a ‘cataclysmic peak’ into the impact rate function in the form of a Gaussian component. The occurrence times for the basin-forming events are recalculated from the N(20) crater density table according to the cumulative form of this function (Figure 17b,c), causing them to be compressed in time either partially (Figure 19a) or fully (Figure 19b) into the narrow interval of the peak. In the results, the peak is rather precisely reflected in the presence of melt from that time throughout the depth range. It could be expected that other basin events would have occurred before these, but since they would not now be observable, they are not included in the table. This is likely in the non-cataclysm scenario as well.

4.4 Discussion

The predictions of the model should be understood within the context of the simplifying assumptions used in its construction. Some of the more significant among these are described below.

We take no account of other internal processes (volcanism, geothermal heating), and the surface is taken to be homogeneous, so that there is no influence of the mare. Alternative modes of resetting radiometric ages may leave their signature at depth, and this material may also be recycled to the surface through impact gardening.

The crater production function is taken to have been unchanging over the lunar history. If it had a different form in the early observable history, we believe the consequence for our results would not be great: in such a case, we would expect the large-diameter end of the size–frequency distribution described by the Neukum production function to better reflect the early impactor flux, and the small-diameter end to better reflect the later flux. The lasting effect of the small-diameter tail from the early time is small: it is the large events which dominate the melt evolution. In recent time, the small events are important for the final gardening of the uppermost layers of the regolith, while the large events have become so sparse in time that they no longer have an influence. Nevertheless, different scenarios for variation of the production function would change the detail of the outcome.

Placing the basin formation times according to the Neukum chronology model using observed N(20) values brings about a spread of basin ages from 3.8-4.2 Ga. We expect that the measurements of N(20) for older basins are diminished with respect to the count of craters which actually formed on the surfaces because of obliteration and non-sparseness effects (Kneissl et al., 2016). It could appear that the episode of basin formation thus constructed is itself a form of cataclysm. We, however, take this as our definition of the non-cataclysm scenario: that is to say that the basin formation is consistent with the Neukum rate function without an additional spike. The fact that the observed basins then occur between 3.8 and 4.2 Ga is not understood by us to represent a cataclysmic period of 400 Ma. We interpret the upper limit at 4.2 Ga to be a horizon beyond which we cannot see: these basin forming events were continuous with others which we are unable to observe. Although the plotted rate function extends backwards beyond the last basin, it is no more than an extrapolation: we can identify no surfaces older than SPA so this portion is also beyond the horizon of observability. It is apparent that the extrapolation, at least for the basin forming flux, cannot be valid back to 4.5 Ga because the accumulated mass would exceed that of the Moon (Ryder, 2002; Zellner, 2017).

We do not consider the depth of melt production: larger impacts produce melt at greater depth, which may be less distributed at the surface. This may lead to an exaggeration of the presence of basin melt at the surface in the model.

The understanding of ‘melt’ as used in this simulation differs from the term as applied in a petrological classification. Here it is understood as the fraction of material which has been heated above a certain threshold. The subsequent history of a particular sample may not necessarily leave it in a state where it remains identifiable as melt: extreme pulverisation may yield a mix which is no longer appears as melt, nor offers the possibility of radiometric dating of the event which produced it. At this point of investigation, therefore, although the calculated numerical quantities are based on reasonable estimates, we expect that there are processes and effects which may cause the actual abundances to be at variance with our predictions. Nevertheless, an important result is the demonstration of the interaction of the influence of both large and small impact events in the lunar history, and the general shape of the resulting melt distribution with depth, which is the outcome of the impact gardening mixing process, and which we believe to be accurate in its general features. The simulation shows that it is statistically reasonable to expect to find melt components surviving from the

basin forming impacts in surface samples today and, further, that they should be the most abundant melt components aside, possibly, from those arising from the very most recent impact events near the sampling site.

The modelling shows that there remains a significant fraction of the lunar material at all depths which is not heated during the period of simulation. Actual samples contain possibly small homogeneous components which are identifiable as melt and are thus separable for dating. A larger fraction of the sample material is not separable in this way, but should – according to our model – have last been heated at earlier times than the identifiable melt components. Hartmann (2003) has hypothesised that impact induced pulverisation may preferentially diminish the oldest melt samples to the point of being undetectable, which would explain why we do not see this older fraction represented in the samples. The pulverised material of surface samples could thus, in part, correspond to the 'unheated material' of the model. We do not date it because there are no components large enough to do so. Chapman et al. (2007) argue, and we agree with them, that pulverisation should be an important process only close to the surface, thus opening the possibility that future samples obtained from greater depth may offer a view further back in to the lunar impact history.

We interpret from our modelling that, if there was a lunar cataclysm or a late heavy bombardment, its form should be observable today in the histogram of melt ages from surface samples, both those returned from the Moon by manned and unmanned spacecraft and those delivered to the Earth in the form of meteorites. Such a feature is not observed in the lunar meteorite histogram, which we consider to be a random sampling of the lunar surface, suggesting that the lunar cataclysm hypothesis is likely false. Furthermore, we show that, in a scenario with no cataclysm, melt from Imbrium is expected to be more abundant than that of any other age near-surface samples.

We believe our summary of K-Ar datings combined with the modelling results contradicts the idea of a short terminal cataclysm. If we place the basin events at times as predicted by the Neukum model according to their N(20) values we find the results of the modelling generally consistent with the lunar meteorite age distribution, and suggest the variations seen in returned samples are local effects. What happens prior to the visible basins is less clear. We do not see the component of material which is unheated throughout the simulation in samples, which should be at least 4.2 Ga old. We attribute this to the pulverisation effect: the material

is present, but not possible to date. It may be that this occurs only for near-surface samples, and that future missions aimed to obtain samples from low-lying outcrops might allow us to see further back. If the choice of time points for basin formation is even roughly valid, it is evident that their frequency increases going back in time. It is not unreasonable to think that this continues backwards beyond the oldest basins we see, but it must eventually be constrained by the mass of the system. The exponential decay of the Neukum extrapolation makes sense so long as the dominant process is the removal of projectiles from the system by collision with the Moon or other established bodies. When – going backwards – the number of projectiles becomes sufficiently high that interaction between projectiles is significant, we could expect a different form of decay. We suggest this has to occur in a way which leads to a lesser rate of impact of large bodies than would be predicted by the exponential curve.

We intend, in future work, to extend the model to consider the distribution of melt over the lunar surface, as well as by depth, estimating the melt production and ejecta dispersion from hydrodynamic models of different scales. We aim to understand the lateral transport of melt components driven by impact gardening. More generally, this type of modelling may eventually permit the inversion the observed melt age histogram to obtain new constraints on the impact rate function, a potential new approach to the calibration of the lunar cratering chronology system.

5. General discussion and conclusions

The aim of our work was to consider whether the so-called ‘lunar terminal cataclysm’ actually occurred. The phenomenon is understood as a strong peak in the bombardment of the Moon taking place around 3.9 Ga ago, leading to the formation of most of the impact craters observed on the lunar highlands and thus the majority of lunar highland impact breccias and melts. The hypothesis, suggested by Tera et al. (1973, 1974), was based on the observation that the ages of highland samples returned from all the lunar missions, and determined by a variety of isotopic techniques, show a grouping around 3.9–4.0 Ga. Since then, dating techniques have progressed and many old and new samples have been re-analyzed, but the debate over whether the terminal cataclysm occurred has endured.

To progress in the issue, we summarized the results of 269 K-Ar datings of highland rocks represented by the Apollo 14, 15, 16, 17 and Luna 20 samples and 94 datings of clasts of highland rocks from 23 lunar meteorites representing 21 randomly distributed localities on

the lunar surface. We considered these jointly with results of a new model of the cumulative effect of the impact gardening process on the presence of impact melt of different ages at the near-surface of the Moon.

The aggregated results of K-Ar dating of the Apollo-Luna samples of lunar highland rocks reconfirmed the presence of a strong peak centered on 3.87 Ga. The modelling showed that we should indeed expect to see the signature of a late peak in bombardment if it compressed the formation period of the basins observed today. Its prediction, indeed, is that the signature should be a universal feature of collections of near-surface samples.

The 3.87 Ga peak is the only prominent feature at the Apollo 14 and 15 sites, but the age pattern is more complicated at the Apollo 16 and 17 sites. At the same time, the distribution of K-Ar ages for the highland rocks of lunar meteorites, which we consider to be a spatially random sampling of the near-surface of the lunar highlands, shows no such peak, which appears inconsistent with the terminal cataclysm hypothesis.

We favour an interpretation where the discrepancy results from sampling bias: where the peak is the only prominent feature, the sites are likely dominated by Imbrium basin ejecta (Apollo 14 and 15), and those with a more complex signature likely influenced by the ejecta of Nectaris (Apollo 16) and Serenitatis (Apollo 17). The Imbrium impact was the largest among the late basin-forming events, influencing all the areas sampled by Apollo 14, 15, 16, 17 and Luna 20. Indeed, in the sense of the production of impact melts and brecciation, it could be considered a kind of ‘local’ terminal cataclysm.

As follows from common intuition and was confirmed by our modeling, a cataclysm should lead to a peak in the frequency of measured age values. In the aggregated histograms and relative probability plots we observe a 3.87 Ga peak, which we attribute to the Imbrium event, and a few secondary peaks caused by the formation of other basins in the vicinity.

Thus, our general conclusion is that the terminal cataclysm proposed by Tera et al. (1973, 1974) as a strong peak in meteorite bombardment of the Moon, when most of the craters observed in lunar highlands and thus most of the lunar highland impact breccias were formed, did not occur. We see evidence of the formation of several impact basins between 3.87 to 4.25 Ga and there remain other observed basins, including the largest South Pole – Aitken, the ages of which should be determined in future studies. Special sample-return missions targeted to date several key basins need to be planned. Further studies of lunar meteorites may also bring new details to the general picture of the impact bombardment of the Moon.

Acknowledgements: We are grateful to Boris Ivanov and Tomokatsu Morota for their careful reviews of the manuscript and acknowledge discussions with H. Becker, V. Fernandes, T. Kneissl, E. Korochantseva, Yu. Kostitsyn, and T. Liu. The work was supported by the German Space Agency (DLR Bonn), grant 50QM1702 (HRSC on Mars Express), on behalf of the German Federal Ministry of Economics and Technology, and by the German Research Foundation (DFG) SFB TRR-170 A4.

References

Baksi A. K., Archibald D. A. and Farrar E. 1996. Intercalibration of 40Ar/39Ar dating standards. Chem. Geol. 129, 307–324.

Baldwin, R. B., 1974. Was there a 'terminal lunar cataclysm' 3.9 to 4.0 billion years ago? Icarus, 23, 157-166

Basilevsky, A.T., Neukum, G., 2010. Are all lunar highland pristine rocks really pristine? Nördlingen 2010: The Ries Crater, the Moon, and the Future of Human Space Exploration, 7015 (abstract).

Boehnke P., Harrison T.M., 2016. Illusory Late Heavy Bombardments. Proceedings of the National Academy of Sciences of USA; www.pnas.org/cgi/doi/10.1073/pnas.1611535113

Bogard D.D., 1995. Impact ages of meteorites: A synthesis. Meteoritics. V. 30. 244-268.

Bogard D.D., 2011. K–Ar ages of meteorites: Clues to parent-body thermal histories. Chemie der Erde. 71. 207–226.

Bogard D. D., Harrison D. H. and Nyquist L. E. (2000) Argon-39-Argon-40 Ages of lunar highland rocks and meteorites. Lunar Planet. Sci. 31, #1138.

Bogard D.D. and Harrison D.H., 2003. 39Ar-40Ar ages of eucrites and thermal history of asteroid Vesta. Meteoritics and Planetary Science. V. 38. Nr 5. 669-710.

Bogard D.D., Nyquist L.E., Bansal B.M., Wiesmann H. and Shih C.-Y. (1975) 76535: An old lunar rock. *Earth Planet. Sci. Lett.* 26, 69-80.

Bottke, W.F., Levison, H.F., Nesvorný, D., Dones, L., 2007. Can planetesimals left over from terrestrial planet formation produce the lunar Late Heavy Bombardment? Icarus 190, 203–223.

Bottke W.F., Vokrouhlicky D., Minton D., Nesvorny D., Morbidelli A., Brasser R., Simonson B., Levison H.F., 2012. An Archaean heavy bombardment from a destabilized extension of the asteroid belt. Nature, V. 485, 78-81.

Cadogan P.H., Turner G (1977) 40Ar-39Ar dating of Luna 16 and Luna 20 samples. Phil Trans Royal Soc London 284: 167-177

Chapman C. R., Cohen B. A., Grinspoon D. H. 2007. What are the real constraints on the existence and magnitude of the late heavy bombardment? Icarus, 189, 233-245.

Chapman P. K., Calio A. J., Simmons M. G. (1971) Summary of scientific results. In: Apollo 14 Preliminary Science Report, NASA SP-272, Washington, D.C., 1-8.

Cintala, M.J., Grieve, R.A.F. (1998) Scaling impact melting and crater dimensions: Implications for the lunar cratering record. Meteorit. Planet. Sci. 33, 889–912.

Culler et al (2000) Lunar Impact History from 40Ar/39Ar Dating of Glass Spherules. Science. 287, 1785-1788.

Cohen, B.A. (2008) Lunar meteorite impact melt clasts and lessons learned for lunar surface sampling. Lunar Planet. Sci. XXXIX, #2532.

Cohen B. A., Swindle T. D., and Kring D. A. (2000) Support for the Lunar Cataclysm Hypothesis from Lunar Meteorite Impact Melt Ages. *Science* **290**, 1754-1756.

Cohen B. A., Swindle T. D., Kring D. A. and Olson E. K. (2005) Geochemistry and 40Ar39Ar geochronology of impact-melt clasts in lunar meteorites Dar al Gani 262 and Calcalong Creek. *Lunar Planet. Sci.* **36**, #1481.

Cohen B. A., Swindle T.D., Taylor L.A. and Nazarov M.A. (2002) 40Ar-39Ar ages from impact melt clasts in lunar meteorites Dhofar 025 and Dhofar 026. *Lunar Planet. Sci.* **33**, #1252.

Cohen B. A., Swindle T. D., Kring D. A. and Olson E. K. (2005) Geochemistry and 40Ar39Ar geochronology of impact-melt clasts in lunar meteorites Dar al Gani 262 and Calcalong Creek. *Lunar Planet. Sci.* **36**, #1481.

Das, J. P.; Baldwin, S. L.; Delano, J. W. 2016. ^{40}Ar/^{39}Ar and cosmic ray exposure ages of plagioclase-rich lithic fragments from Apollo 17 regolith, 78461. Earth, Planets and Space,. Volume 68, article id.11, 15 pp

Daubar I. J., Kring D. A., Swindle T. D., and Jull A. J. T. (2002) Northwest Africa 482: A crystalline impact-melt breccia from the lunar highlands. *Meteorit. Planet. Sci.* **37**, 1797-1814.

Duncan, R.A., Norman, M.D., 2005. Assembly of the Descartes terrane: argon ages of lunar breccias 67016 and 67455. Meteorit. Planet. Sci. 40, A41, abstract.

Eugster O., Geiss J., Krähenbühl U. and Niedermann S. (1986) Nobel gas isotopic composition, cosmic ray exposure history, and terrestrial age of the meteorite Allan Hills A81005 from the Moon. *Earth Planet. Sci. Lett*. 78, 139-147.

Fassett, C.I., Head J.W., Kadish S.J., Mazarico E., Neumann G.A., Smith D.E., Zuber M.T., 2012. Lunar impact basins: Stratigraphy, sequence and ages from superposed impact crater populations measured from Lunar Orbiter Laser Altimeter (LOLA) data. Journal of Geophysical Research (Planets). V. 117. E00H06.

Fassett C.I. and Minton D.A. Impact bombardment of the terrestrial planets and the early history of the Solar System. Nature Geoscience. 2013. V. 6. 520-524. DOI: 10.1038/NGEO1841

Fernandes V.A., Burgess R., Turner G. (2000) Laser argon-40-argon-39 age studies of Dar al Gani 262 lunar meteorite. Meteoritics and Planetary Science. 35. 1335-1364.

Fernandes V.A., Anand M., Burgess R., and Taylor L. A. (2004) Ar-Ar studies of Dhofar clast-rich feldspathic highland meteorites: 025, 026, 280, 303. *Lunar Planet. Sci.* 35, #1514.

Fischer-Gödde, M. and Becker H. (2011) What is the age of the Nectaris basin? New Re-Os constraints for a pre=4.0 Ga bombardment history of the Moon. LPSC-42, abs. 1414.

Flude, S., Halton, A., Kelley, S., Sherlock, S., Schwanethal, J. & Wilkinson, C. 2014. Observation of centimetre scale argon diffusion in alkali feldspars: implications for 40Ar/39Ar thermochronology. In: Jourdan, F., Mark, D. F. & Verati, C. (eds) Advances in 40Ar/39Ar Dating: from Archaeology to Planetary Sciences. Geological Society, London, Special Publications, 378. 265-275. http://dx.doi.org/10.1144/SP378.25.

Frey H.V., 2016. Comparing the Early and Late Heavy bombardments on the Moon. LPSC-47. Abs. 1238.

Geiss, J., Rossi, A.P., 2013. On the chronology of lunar origin and evolution. Implications for Earth, Mars and the Solar System as a whole. The Astronomy and Astrophysics Review, Volume 21, article id.68

Gomes, R., Levison, H.F., Tsiganis, K., Morbidelli, A., 2005. Origin of the cataclysmic late heavy bombardment period of the terrestrial planets. Nature 435, 466–469.

Grieve, R.A.F., Stöffler, D., Deutsch, A. (1991) The Sudbury structure: Controversial or misunderstood? J. Geophys. Res. 96, 22753–22764.

Haber T., Norman M. D., Bennett V.C. and Jourdan F., 2014. Formation ages, cogenetic relations and formation processes of a set of Apollo 16 impact melt rocks. LPSC-45. Abs. 1693.

Hartmann, W.K. 1965. Secular changes in meteoritic flux through the history 0fv the Solar system. Icarus. 4, 207-213.

Hartmann, W.K. 1966. Early lunar cratering. Icarus. 5, 406-418.

Hartmann, W.K. 1972. Paleocratering of the Moon: Review of post-Apollo data. Astrophys. Space Sci. 12, 48-64.

Hartmann, W.K. 2003. Megaregolith evolution and cratering cataclysm models – Lunar cataclysm as a misconception (28 years later). Meteoritics and Planetary Science 38, 4, 579-593.

Hartmann W. K., Quantin C., Mangold N. 2007. Posible long-term decline in impact rates. 2. Lunar impact-melt data regarding impact history. Icarus, 186, 11-23.

Hinners N. W. (1972) Apollo 16 site selection. In: Apollo 16 Preliminary Science Report, NASA SP-315 Washington, D.C., pp. 1-1 – 1-3.

Hörz, F., Ostertag, R., Rainey, D.A., 1983. Bunte Breccia of the Ries: Continuous deposits of large impact craters. Reviews of Geophysics 21, 1667–1725.

Husain L., Schaeffer O.A. and Sutter J.F. (1972a) Age of a lunar anorthosite. Science 175, 428-430.

Joy K. H., Burgess R., Hinton R., Fernandes V. A., Crawford I. A., Kearsley A. T., and Irving A. J., 2011. Petrogenesis and chronology of lunar meteorite Northwest Africa 4472: A KREEPy regolith breccia from the Moon. Geochimica et Cosmochimica Acta 75:2420–2452.

Jourdan, F., Mark, D. F., Verati, C, 2014. Advances in 40Ar/39Ar Dating: from Archaeology to Planetary Sciences. Geological Society, London, Special Publications. 378, 1–8. https://doi.org/10.1144/SP378.24.

Kaneoka, I. and Takaoka,N (1986) 40Ar-39Ar analyses of an Antarctic meteorite Yamato-791197 of probable lunar origin. *Mem. Natl. Inst. Polar Res., Spec. Iss.* **41**, 116 123.

Kneissl, T., Michael, G.G., Schmedemann, N., 2016. Treatment of non-sparse cratering in planetary surface dating. Icarus 277, 187–195.

Korochantseva E. V., Trieloff M., Hopp J., Buykin A. I., and Korochantsev A. V. (2009) 40Ar-39Ar dating of solar gas-rich lunar meteorite Dhofar 1436 (abstract). 72th Annual Meeting of the Meteoritical Society, number 5226.

Korochantseva E.V., Buikin A.I., Hopp J., Korochantsev A.V., and Trieloff M. (2016) 40Ar-39Ar results of lunar meteorites Dhofar 025, 280, 309, 730, 733, 1436, 1442, SAU 449, NWA 6888. 79th Annual Meeting of the Meteoritical Society, number 6317.

Korochantseva E.V., Buikin A.I., Hopp J., Korochantsev A.V., and Trieloff M. 2016. 40Ar-39Ar dating of lunar meteorites Dhofar 309 and 730. 2016. LPSC-47. Abs. 2305.

Korotev R. L. (1994) Compositional Variation in Apollo 16 Impact-Melt Breccias and Inferences for the Geology and Bombardment History of the Central Highlands of the Moon. Geochimica et Cosmochimica Acta, vol. 58, p. 3931-3969.

LSPET (The Lunar Sample Preliminary Examination Team) (1971) Preliminary examination of lunar samples. In: Apollo 14 Preliminary Science Report, NASA SP-272, Washington, D.C., pp. 109-132.

LSPET (The Lunar Sample Preliminary Examination Team) (1972) Preliminary examination of lunar samples. In: Apollo 15 Preliminary Science Report, NASA SP-289, Washington, D.C., pp. 6-1 – 6-25.

LSPET (The Lunar Sample Preliminary Examination Team) (1973) Preliminary examination of lunar samples. In: Apollo 17 Preliminary Science Report, NASA SP-315, Washington, D.C., pp. 7-1 – 7-24.

Marchi S., Bottke W.F., Cohen B.A., Wünnemann K., Kring D.A., McSween H.Y., De Sanctis M.C., O'Brien D.P., Schenk P., Raymond C.A., Russell C.T. High-velocity collisions from the lunar cataclysm recorded in asteroidal meteorites. Nature Geoscience. 2013. V. 6. 303-307. DOI: 10.1038/NGEO1769

Maurer P., Eberhardt P.. Geiss J., Groegler N., Stettler A., Brown G. M., A. Peckett, Kraehenbuehl U. (1978) Pre-Imbrian craters and basins: ages, compositions and excavation depths of Apollo 16 breccias. Geochim. Cosmochim Acta, 1978, 42, 1687-1720.

McDougall I. and Harrison T.M. Geochronology and Thermochronology by the 40Ar/39Ar Method. Oxford University Press. Second Edition. 1999. 288 p.

McKinnon, W.B., Zahnle, K.J., Ivanov, B.A., Melosh, H.J., 1997. Cratering on Venus: Models and Observations, in: Bougher, S.W., Hunten, D.M., Phillips, R.J. (Eds.), VenusIIGeology,Geophysics,Atmosphere, Solar Wind Environment. p. 969.

McLeod, Claire L.; Brandon, Alan D.; Fernandes, Vera A.; Peslier, Anne H.; Fritz, Jörg; Lapen, Thomas; Shafer, John T.; Butcher, Alan R.; Irving, Anthony J. Constraints on formation and evolution of the lunar crust from feldspathic granulitic breccias NWA 3163 and 4881. Geochimica et Cosmochimica Acta, 2016. Volume 187, p. 350-374.

Melosh, H.J., 1989. Impact Cratering: A Geologic Process. Oxford University Press, New York. 256 p.

Michael, G.G., Kneissl, T., Neesemann, A., 2016. Planetary surface dating from crater size-frequency distribution measurements: Poisson timing analysis. Icarus 277, 279–285.

Morbidelli A, Marchi S, Bottke WF, Kring DA (2012) A sawtooth-like timeline for the first billion years of lunar bombardment. Earth Planet Sci Lett 355-356:144–151.

Morrison, D.A. (1998) Did a thick South Pole-Aitken basin melt sheet differentiate to form cumulates? Lunar Planet Sci. XXIX, abs.1657.

Muehlberger W.R., Batson R. M., Boudette E. L., Duke C. M., Eggleton R. E., Elston D. P., England A. W., Freeman V. L., Hait M. H., Hall T. A., Head J. W., Hodges C. A., Holt H. E., Jackson E. D., Jordan J. A., Larson K. B., Milton D. J., Reed V. S., Rennilson J. J., Schaber G. G., Sehafer J. P., Silver L. T., Stuart-Alexander D., Sutton R. L., Swann G. A., Tyner R. L., Ulrich G. E., Wilshire H. G., Wolfe E., and Young J. (1973) Preliminary geologic investigation of the Apollo 16 landing site In: Apollo 16 Preliminary Science Report, NASA SP-315, Washington, D.C., pp. 6-1 – 6-81.

Muehlberger W. R., Batson R. M., Cernan E. A., Freeman V. L., Halt M. H., Holt H. E., Howard K. A., Jackson E. D., Larson K. B., Reed V. S., Rennilson J. J., Schmitt H. H., Scott D. H., Sutton R. L., Stuart-Alexander D., Swann G. A., Trask J., Ulrich G. E., Wilshire H. G., and Wolfe E. W. (1973) Preliminary geologic investigation of the Apollo 17 landing site. In: Apollo 17 Preliminary Science Report, NASA SP-315, Washington, D.C., pp. 6-1 – 6-91.

Murray B.C., Strom R.G., Trask N.J., Gault D.E. Surface history of Mercury: Implications for terrestrial planets. Journal of Geophysical Research. 1975. V. 80. No 17. 2508-2514.

Mutch T.A., Arvidson R.E., Head J.M. et al. The geology of Mars. Princeton: Univ. press, 1976. 400 p.

Nakamura N., Tatsumoto M., Nunes P.D., Unruh D.M., Schwab A.P. and Wildeman T.R. (1976) 4.4 b.y.-old clast in Boulder 7, Apollo 17: A comprehensive chronological study by U-Pb, Rb-Sr, and Sm-Nd methods. Proc. 7th Lunar Sci. Conf. 2309-2333.

Neukum, G., 1983. Meteoritenbombardement und Datierung planetarer Oberflachen (English translation, 1984: Meteorite bombardment and dating of planetary surfaces. http://ntrs.nasa.gov/search.jsp?R=19840027189).

Neukum G., Ivanov B.A., 1994. Crater size distributions and impact probabilities on Earth from lunar, terrestrial planet, and asteroid cratering data. Hazards Due to Comets and Asteroids. Elsevier Science B.V., Amsterdam. 359-416

Neukum G, König B, Fechting H, Storzer D (1975b) Cratering in the Earth-moon system: Consequences for age determination by crater counting. Proc Lunar Sci Conf 6:2597-2620

Norman M. D., Duncan R. A., Huard J. J. (2006) Identifying impact events within the lunar cataclysm from 40Ar–39Ar ages and compositions of Apollo 16 impact melt rocks. Geochimica et Cosmochimica Acta 70 (2006) 6032–6049

Norman M.D., Duncan R.A., Huard J.J. (2010) Imbrium provenance for the Apollo 16 Descartes terrain: Argon ages and geochemistry of lunar breccias 67016 and 67455 Geochim. et Cosmochim. Acta 74 763–783

Norman, M.D., Nemchin, A.A. 2014. A 4.2 billion year old impact basin on the Moon: U-Pb dating of zirconolite and apatite in lunar melt rock 67955ю. Earth and Planetary Science Letters, Volume 388, p. 387-398.

Norman, M. D.; Taylor, L. A.; Shih, C.-Y.; Nyquist, L. E. 2016. Crystal accumulation in a 4.2 Ga lunar impact melt. Geochimica et Cosmochimica Acta, V. 172. 410-429.

Nyquist L., Bogard D., Yamaguchi A., Shih C.-Y., Karouji Y., Ebihara M., Reese Y., Garrison D., Takeda H. (2006) Feldspatic clasts in Yamato 86032: remnants of the lunar crust with implication for its formation and impact history. *Geochim. Cosmochim. Acta* 70(24). 5990-6015.

Nyquist L. E., Shih C.-Y., Reese Y. D. (2011)Dating melt rock 63545 by Rb-Sr and Sm-Nd: age of Imbrium; SPA dress rehearsal. Lunar and Planetary Science 42, abs. 1868

Papanastassiou D.A, Wasserburg GJ (1972) The Rb-Sr age of a crystalline rock from Apollo 16. Earth Planet Sci Lett 16:289-298

Park J., Nyquist L.E., Herzog G.F., Turrin B.D., Lindsay F.N., Delaney J.S., Swisher III C.C.. Shih C.-Y., Yamaguchi A., 2015. Newly determined Ar/Ar ages of lunar troctolite 76535. LPSC-46. Abs. 2018.

Park J., L. Nyquist E., Shih C.-Y., Herzog G.F., Yamaguchi A., Shirai N., Ebihara M., Lindsay F.N., Delaney J., Turrin B., Swisher III C.C. (2013) Late Bombardment of the Lunar Highlands Recordeded in MIL 090034, MIL 090036 and MIL 090070 Lunar Meteorites. 44th Lunar and Planetary Science Conference. Abs. 2576.

Pike, R.J., 1980. Control of crater morphology by gravity and target type - Mars, earth, moon, in: Bedini, S.A. (Ed.), Lunar Planetary Science Conference Proceedings, Lunar Planetary Science Conference Proceedings. pp. 2159–2189.

Prettyman T. H, Hagerty J. J., Elphic R. C., Feldman W. C., Lawrence D. J., McKinney G. W., Vaniman D. T. (2006) Elemental composition of the lunar surface: Analysis of gamma ray spectroscopy data from Lunar Prospector. J. Geophys. Res. 111, E12007, doi:10.1029/2005JE002656.

Renne P. R., Swisher C. C., Deino A. L., Karner D. B., Owens T. L. and DePaolo D. J. (1998) Intercalibration of standards, absolute ages and uncertainties in 40Ar/39Ar dating. Chem. Geol. 145, 117–152.

Ryder, G., 2002. Mass flux in the ancient Earth-Moon system and benign implications for the origin of life on Earth. Journal of Geophysical Research: Planets 107, 6–1–6–13.

Schaeffer O. A. and Husain L. (1973) Early lunar history: Ages jf 2 to 4 mm soil fragments from the lunar highlands. Proc. Fourth Lunar Sci. Conf., v.2, 1847-1863.

Schmedemann N., Kneissl T., Ivanov B.A. and 16 coauthors, 2014. The cratering record, chronology and surface ages of (4)Vesta in comparison to smaller asteroids and the ages of HED meteorites. Planetary and Space Science. V. 103. 104–130.

Schmitt, H.H. Evolution of the Moon: The 1974 Model. In: The Soviet-American Conference on Cosmochemistry of the Moon and Planets, Edited by J.H.Pomeroy and N.J.Hubbard. NASA Administration, Washington, D.C. 1977. p.63-80.

Spudis P. and Pieters C. (1991) Global and regional data about the Moon. In: Lunar Source Book. A User Guide to the Moon. Heiken, G.H., Vaniman, D.T., French, B.M. (Eds.), Cambridge Univ. Press, 595-632.

Spudis P.D., Ryder G. (1981) Apollo 17 impact melts and their relations to the Serenitatis basin. In: Schultz P.H. and Merrill R.B., eds., Multiring Basins: Proceedings, Lunar and Planetary Science 12A, 133-148.

Spudis P.D., Wilhelms D.E., Robinson M.S. (2011) Sculptured Hills: Implications for the relative age of Serenitatis, basin chromologies and the cratering history of the Moon. LPSC-42, abs.1365.

Steiger R.H. and Jaeger E. 1977.Subcommission on geochronology: Convention on the use of decay constants in geo- and cosmochronology. Earth Planet. Sci. Lett, 36,359-362.

Stettler A., Eberhardt P., Geiss J., Grogler N. and Guggisberg S. (1978) Chronology of the Apollo 17 Station 7 Boulder and the South Serenitatis impact (abs). Lunar Planet. Sci. IX, 1113-1115. Lunar Planetary Institute, Houston.

Stoeffler D., Bischoff A., Borchardt R., Burghele A., Deutsch A., Jessberger E. K., Ostertag R., Palme H., Spettel B., Reimold W. U., Wacker K., Waenke H. (1985) Composition and evolution of the lunar crust in the Descartes highlands, Apollo 16. In:. 15th Lunar Planet. Sci. Conf. Proc. Part 2, pp. C449-C506.

Swann G.A., Bailey N.G.. Batson R.M., Freeman V.L., Hair M.H., Head J. W., Holt H.E., Howard K.A.. Irwin J.B., Larson K.B., Muehlberger W.R., Reed V.S., Rennilson J.J., Schaber G.G., Scott D.R., Silver L.T., Sutton R.L. G.E. Ulrich, H.G. Wilshire, and E. W. Wolfe (1972) Preliminary geologic investigation of the Apollo 15 landing site. In: Apollo 15 Preliminary Science Report, NASA SP-289, Washington, D.C., pp. 5-1 – 5-112.

Takeda H., Yamaguchi A., Bogard D. D., Karouji Y., Ebihara M., Ohtake M., Saiki K. and Arai T. (2006) Magnesian anorthosites and a deep crustal rock from the farside crust of the moon. *Earth and Planetary Science Letters* **247**, 171-184.

Taylor, G.J., Warren, P., Ryder, G., Delano, J., Pieters, C., Lofgren, G. 1991. Lunar rocks. In: Lunar Source Book. A User Guide to the Moon. Heiken, G.H., Vaniman, D.T., French, B.M. (Eds.), Cambridge Univ. Press, 183-284.

Tera F, Papanastassiou DA,Wasserburg GJ (1976) Lunar ball games and other sports. Lunar Planet Sci VII: 858-860

Tera F, Papanastassiou DA, Wasserburg GJ (1974) Isotopic evidence for a terminal lunar cataclysm. Earth Planet Sci Lett 22:1-21

Thomas P.C., Binzel R.P., Gaffey M.J., Storrs A.D., Wells E.N., Zellner B.H. 1997. Impact excavation on asteroid 4 Vesta: Hubble Space Telescope results. Science, V. 277. 1492-1495.

Turner G (1977) Potassium-argon chronology of the Moon. Phys Chem Earth 10:145-195

Turner, G., Cadogan, P.H., Yonge, C.J. (1973). Argon selenochronology. Proc. Lunar Sci. Conf. 4th. V. 2, 1889-1914.

Turner G., Huneke J.C., Podosek F.A. and Wasserburg G.J. (1972) Ar40-39 systematics in rocks and separated minerals from Apollo 14. Proc. 3rd Lunar Sci. Conf. 1589-1612.

Vaughan W.M., Head J.W., Wilson L., Hess P.C. (2013) Geology and petrology of enormous volumes of impact melt on the Moon: A case study of the Orientale basin impact melt sea. Icarus 223 749–765

Wartho, J.-A., Kelley, S. P. & Elphick, S. C. 2014. Ar diffusion and solubility measurements in plagioclases using the ultra-violet laser depth-profiling technique. In: Jourdan, F., Mark, D. F. & Verati, C. (eds) Advances in 40Ar/39Ar Dating: from Archaeology to Planetary Sciences. Geological Society, London, Special Publications, 378. 137-154. http://dx.doi.org/10.1144/SP378.13

Wilhelms, D. E. with sections by McCauley J.F. and Trask N.J., 1987. The geologic history of the Moon. U.S. Geol. Surv. Prof. Paper, Report P 1348, 302 p., 12 plates.

Zellner, N.E.B., 2017. Cataclysm No More: New Views on the Timing and Delivery of Lunar Impactors. Origins of Life and Evolution of the Biosphere.